

**UNIVERSITY
OF OULU**

FACULTY OF TECHNOLOGY

U-Pb zircon dating of metasedimentary rocks within the Ikkari gold deposit, Central Lapland belt, northern Finland

Samuli Harju

MASTER'S PROGRAMME IN GEOSCIENCE

Master's thesis

2022

TIIVISTELMÄ OPINNÄYTETYÖSTÄ

Tutkimusyksikkö Oulun yliopisto teknillinen tiedekunta	Tutkinto-ohjelma Geologian ja mineralogian koulutusohjelma		
Tekijän nimi Harju, Samuli Aleksi	Työn ohjaaja yliopistolla Ranta, Jukka-Pekka		
Työn nimi U-Pb ikämääritys Ikkarin kultaesiintymän metasedimenttikivien zirkoneista, Keski-Lapin vyöhykkeellä, Pohjois-Suomessa			
Opintosuunta Geotieteet	Työn laji Pro Gradu	Aika Joulukuu 2022	Sivumäärä 41 s., 3 liitettä
Tiivistelmä <p>Ikkarin kultaesiintymä sijaitsee Keski-Lapin vyöhykkeellä, lähellä Jeesiön ja Rajalan kylä. Keski-Lapin vyöhyke koostuu kuudesta stratigrafisesta yksiköstä, vanhimmasta nuorimpaan Sallan ryhmä, Kuusamon ryhmä, Sodankylän ryhmä, Savukosken ryhmä, Kittilän sviitti ja Kummun ryhmä. Tutkimuksen tarkoituksena oli selvittää, Ikkarin metasedimenttien ikäjakauma ja mihin stratigrafiseen yksikköön ne kuuluvat. Ikämääritykset tehtiin metasedimenteissä olevista detritaalisista zirkoneista zirkon U-Pb menetelmän avulla ja näitä ikämääritystuloksia vertailemalla muihin julkaisuihin. Petrografisissa tutkimuksissa tutkittiin ohutleikkien mineraalikoostumus ja kivilaji.</p> <p>Kaksi näytteistä on konglomeraatteja ja kahdeksan serisiitti-albiitti muuttuneita kvartsiitteja. Konglomeraattien suurimmat zirkonipopulaatiot asettuvat noin 2.015 Ga ikään ja niiden maksimi kerrostumisajat ovat 1910 ± 10 Ma (120059_A) ja 1919 ± 5 Ma (120071_A). Luultavasti Savukosken ryhmän ja Kittilän sviitin kivet ovat olleet paikallinen lähde 2.05-2.00 Ga zirkoneille. Kvartsiittien suurimmat zirkonipopulaatiot asettuvat noin 1.95-1.90 Ga ja niiden maksimikerrostumisikä on 1.86-1.90 Ga välillä. Felsinen magmatismi Lapin granuliittivyöhykkeellä on mahdollinen materiaalinlähde näille zirkonipopulaatioille.</p> <p>Verrattaessa työn zirkonipopulaatioita muihin julkaisuihin osoittautuivat kaikki työn näytteet Kummun ryhmän kiviksi, konglomeraattien ollessa kuitenkin hieman vanhempia. Osassa zirkonirakeista on havaittavissa metamorfista ylikasvua.</p>			
Asiasanat: Zirkoni, U-Pb geokronologia, kultaesiintymä, metasedimentti, stratigrafia,			

ABSTRACT FOR THESIS

Research Unit University of Oulu Faculty of Technology		Degree Programme Degree Programme in Geology and Mineralogy	
Author Harju, Samuli Aleksi		Thesis Supervisor Ranta, Jukka-Pekka	
Title of Thesis U-Pb zircon dating of metasedimentary rocks within the Ikkari gold deposit, Central Lapland belt, northern Finland			
Major Subject Geosciences	Type of thesis Master's Thesis	Submission Date December 2022	Number of Pages 41 p., 3 app.
<p>Abstract</p> <p>The gold deposit of Ikkari located in Central Lapland belt, near Jeesiö and Rajala villages. Central Lapland belt have been divided to six units from oldest to youngest: Salla group, Kuusamo group, Sodankylä group, Savukoski group, Kittilä suite and Kumpu group. The purpose of this study was to figure out how old metasediments of Ikkari are and what stratigraphy unit they represent by using U-Pb method to zircon grains and comparing these age results to older publications. Mineralogy and lithology of the samples were studied in petrography studies from thin section.</p> <p>Two of the samples are conglomerates and eight are sericite-albite altered quartzites. Major zircon populations of the conglomerates occur ca. 2.015 Ga and maximum deposit ages of them occur 1910 ± 10 Ma (120059_A) and 1919 ± 5 Ma (120071_A). Rocks of Kittilä suite and Savukoski group are probably the local source for the sedimentary material of this age. Major zircon populations of the quartzites occur ca. 1.95-1.90 Ga and maximum deposit ages of them are between 1.90-1.86 Ga. The felsic magmatism in the Lapland Granulite belt is potential source for the material of this age zircon populations.</p> <p>Based on U-Pb ages of the detrital zircon populations of this study, samples can be correlated in to the Kumpu group. The conglomerates are slightly older than the quartzites. Metamorphic overgrowth occurs in some zircon grains.</p>			
Keywords: Zircon, U-Pb geochronology, gold deposit, metasediment, stratigraphy			

Table of Contents

1. INTRODUCTION	5
2. GEOLOGICAL SETTING	6
2.1. Central Lapland belt	6
2.1.1. Salla group	7
2.1.2. Kuusamo group	8
2.1.3. Sodankylä group	8
2.1.4. Savukoski group	8
2.1.5. Kittilä suite	9
2.1.6. Kumpu group	9
3. FORMATION OF GOLD DEPOSITS AND THEIR OCCURRENCE IN CLB	10
3.1. Formations of gold deposits	10
3.2. Gold occurrences in Central Lapland belt	11
4. ZIRCONS IN GEOCHRONOLOGY AND U-Pb DATING	12
4.1. U-Pb analyses	13
4.2. Metamorphic zircons and alteration of zircons	15
4.3. Use of sedimentary rocks and detrital zircons in age dating	17
4.4. Morphology of zircon grains	18
5. SAMPLING AND ANALYTICAL METHODS	19
5.1. Sampling	19
5.2. Sample preparation	19
5.3. LA-ICPMS Atom	19
6. RESULTS	21
6.1. Petrographic description	21
Conglomerates	21
Quartzites	22
6.2. U-Pb dating	26
120059_A	26
120063_A	26
120071_A	27
120074B_A	27
120094&120097_A	27

120098_A	28
120100_A	28
120112_B.....	28
120112_C.....	29
7. DISCUSSION	33
8. CONCLUSIONS.....	36
9. ACKNOWLEDGEMENTS	37
10. REFERENCES	38

APPENDICES:

Appendix 1. Result of maximum deposition age calculations.

Appendix 2. Morphology of the zircon grains.

Appendix 3. U-Pb analyses.

1. INTRODUCTION

Geochronology is one of the most important tools for studying and understanding evolution of the supracrustal units and its internal stratigraphy. Not only it gives valuable information on the order of deposition of sedimentary and volcanic rocks but can also be used to characterize and uncover the formation processes and timing of ore deposits (Cuney, 2021). Zircon (ZrSiO_4) is one of the most commonly used mineral in geochronological studies (Crowley et al., 2014). When crystallized, zircon incorporates uranium (U) into the crystal structure. Uranium is a radioactive element with two main isotopes ^{238}U and ^{235}U with decay series ending to radiogenic isotopes of lead, ^{206}Pb and ^{207}Pb . During crystallization, zircon incorporates very little Pb, making it ideal tool for dating, as the decay constant of U-isotopes are known (MacDonald, 2013).

Paleoproterozoic supracrustal units within the Fennoscandian shield have been shown to be highly potential for various types of metallic deposits, ranging from ultramafic hosted Ni-Cu-PGE deposit to structurally controlled hydrothermal Au, Au-Cu, Au-Co deposits (Weihed et al., 2008). Understanding of the formational processes and geological evolution of these deposits are challenged by the high metamorphic degree of the rocks and multiple deformation events that have caused complex interference patterns of the lithological units of the area. In those supracrustal areas, Central Lapland belt is one of the most promising metallogenic area within the Fennoscandia with known actively mined mineral deposits, including Europe's largest active gold mine (Kittilä Au mine) along with numerous Au-rich occurrences. The Ikkari Au deposit represent one of those occurrences with preliminary resource estimates of ~4 MoZ Au (Rupert Resources Ltd, 2021).

First signs from Ikkari Au deposit were noticed from base of till research of area in beginning of 2019. First drill hole at the area was drilled in April 2020 which encountered 54m interval with 1.5 g/t Au. The subsequent drilling expanded the known mineralized trend spanning over 500 m wide and including also high gold concentrations (Rupert resources, 2022). First inferred mineral resource estimate for Ikkari published in September 2021 reported 49 million tonnes (Mt) at 2.5 grams per tonne gold (g/t Au) for 3.95 million ounces (Rupert Resources Ltd, 2021). The Ikkari area is located between the Sodankylä and the Kittilä municipalities near Jeesiö and Rajala villages (Figure 1).

In this study, results of U-Pb dating of detrital zircons from the metasedimentary units within the Ikkari Au deposit are reported. The goal is to better characterize the stratigraphical relationships of the different rock units in the area. Work is done in collaboration with University of Oulu and Rupert Finland Oy, subsidiary of the Rupert Resources Ltd.

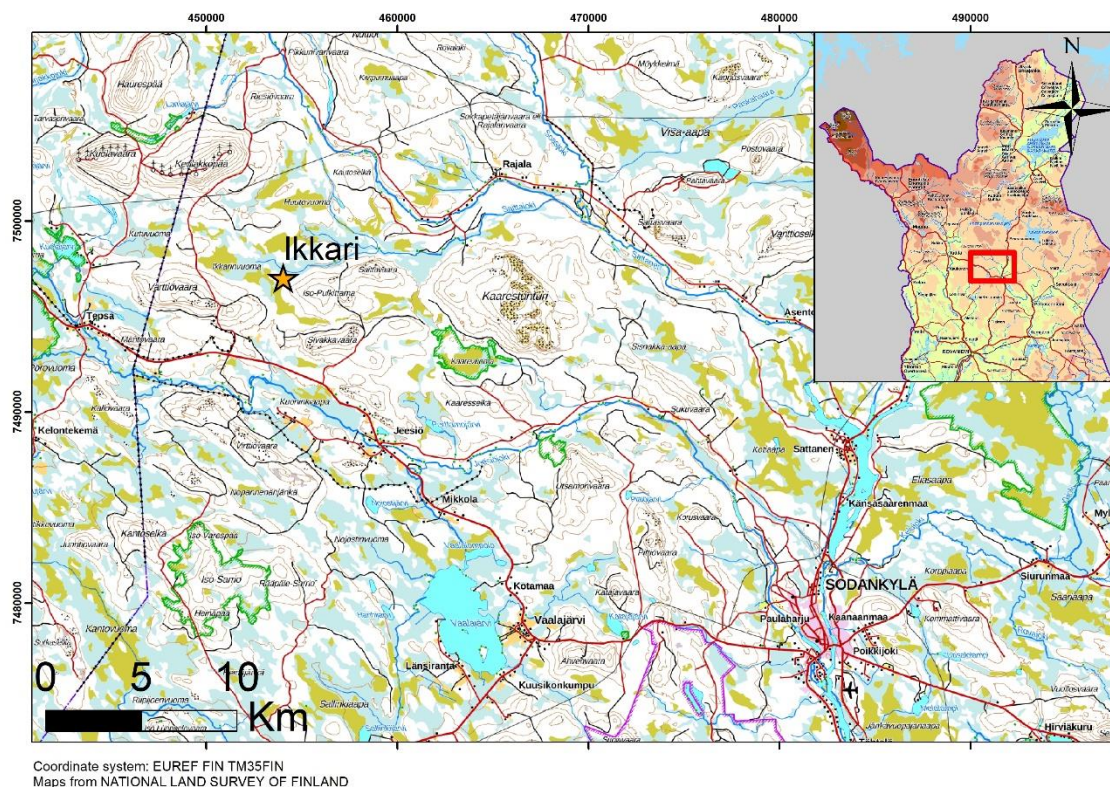


Figure 1. Topographical map showing the location of the Ikkari gold deposit. Inset figure shows the area in more regional context.

2. GEOLOGICAL SETTING

2.1. Central Lapland belt

Central Lapland belt (previously Central Lapland Greenstone Belt) represents Paleoproterozoic supracrustal belt where volcanic and sedimentary units were deposited onto the rifting Archean basement within ca. 600 Ma timeframe between ca. 2.5 Ga and 1.88 Ga (Köykkä et al., 2019). Central Lapland belt have been divided to six units (Figure 2), from oldest to youngest: Salla group, Kuusamo group, Sodankylä group, Savukoski group, Kittilä suite and Kumpu group. The rocks of these groups comprise felsic to ultramafic volcanic rocks and sedimentary units (Hanski and Huhma, 2005), 2.44–2.05 Ga mafic–ultramafic intrusive rocks, 1.92–1.88 Ga felsic porphyritic/lamprophyric rocks,

and 1.88 Ga syn- to 1.80 Ga post orogenic granitoids which are intruded to the supracrustal rocks of CLB (Köykkä et al., 2019).

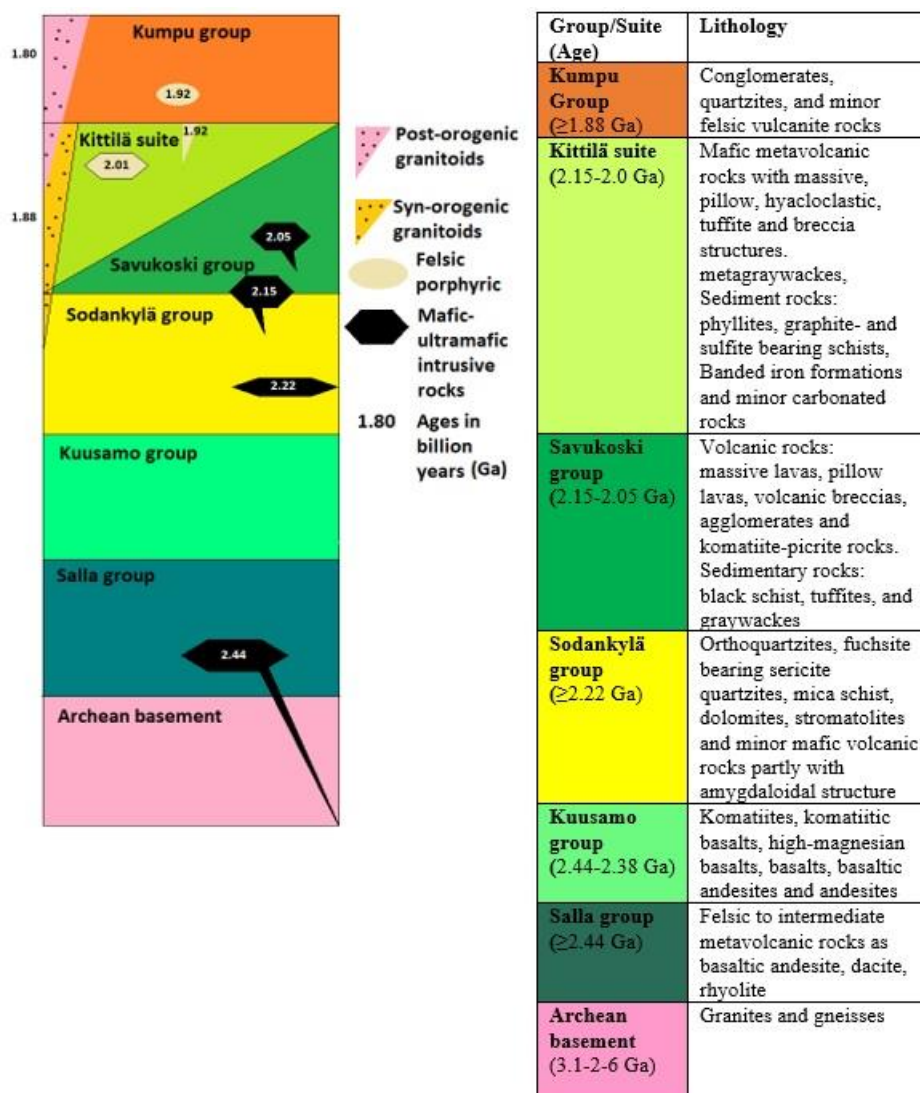


Figure 2. Stratigraphy of Central Lapland Belt, including ages and lithology of units (Modified from Köykkä and Luukas, 2019 and Huhma et al., 2018)

2.1.1. Salla group

Salla group (>2440 Ma; Hanski and Huhma, 2005) is the lowermost and oldest unit in the Central Lapland belt and overlies the Archean basement. The rocks occur in central and eastern part of the belt and are best exposed in the Salla area with outcrops showing primary structures of amygdaloidal volcanic rocks. The composition of the Salla group rocks is varying from intermediate to felsic (basaltic andesites, dacites and rhyolites) and have been metamorphosed under greenschist facies.

2.1.2. Kuusamo group

Former name of the Kuusamo group is Onkamo group (Luukas et al., 2017). Rocks of the Kuusamo group are comprised of ultramafic-mafic to intermediate rocks which are widely spread in Lapland and well exposed in the Salla area (Hanski and Huhma, 2005). Mafic and intermediate lavas are commonly amygdaloidal. Ultramafic rocks are mostly fragmental komatiites. Other extrusive rocks are reported as agglomerates, tuffs, variolitic pillow lavas and pillow breccias, komatiites, andesitic lavas with gneissic xenoliths. On average, the Kuusamo group rocks are more primitive and more varying compared to the Salla group rocks (Hanski and Huhma, 2005). Minimum age of the Kuusamo group is 2383 ± 33 Ma, determined from dike which cut the Kuusamo group volcanic rocks (Hanski and Huhma, 2001). Maximum deposition age of 2405 ± 6 Ma for the Kuusamo group is determined from porphyry clasts of base conglomerate (Köykkä et al., 2019).

2.1.3. Sodankylä group

Sodankylä group rocks are deposited on the top of the Kuusamo group. It consists mainly of sedimentary rocks with minor mafic volcanic rocks (Hanski and Huhma, 2005). The rocks are widely spread on the Central Lapland belt. The Sodankylä group rocks includes sericite quartzites, orthoquartzites, mica schists and dolomites with characteristic stromatolite structures. Green tint is very common feature for sericite quartzites of the Sodankylä group which is due to Cr-bearing mica, fuchsite. Primary textures such as crossbedding, graded bedding, herringbone structures and mud cracks are present in the metasediments (Nikula, 1988). There are also some amygdaloidal structures in mafic volcanic rocks of the Sodankylä group and these usually present few tens of meters thick units (Hanski and Huhma, 2005). These metavolcanic rocks are mainly tholeiitic and basaltic andesite. Some albitization is present also in rocks of the Sodankylä group (Köykkä et al., 2019). Minimum deposition age of the Sodankylä group is 2.22 Ga that is determined from mafic-ultramafic sills cutting the rocks of the Sodankylä group (Huhma et al., 2018).

2.1.4. Savukoski group

Rocks of the Savukoski group overlie the rocks of the Sodankylä group (Hanski and Huhma, 2005). Although these two groups represent different tectonics phases, there is not significant hiatus or discordance between them. The Savukoski group includes black schist and graywackes in bottom parts of the unit, and mafic tuffites and ultramafic volcanics in the upper parts of the unit (Köykkä and Luukas, 2019). The 2.05 Ga age of

the Savukoski group has been determined from diabase dikes which cut the Savukoski group rocks (Huhma et al., 2018). Kevitsa mafic-ultramafic layered intrusion is probably most well-known deposit from the Savukoski group. It is intruded to the bottom part metasediments (Köykkä and Luukas, 2019).

2.1.5. Kittilä suite

Luukas et al., (2017), reclassified the Kittilä group to the Kittilä suite based on poor knowledge of its internal stratigraphy and its allochthonous nature. The Kittilä suite covers over 2600 km² area from the central parts of the Central Lapland belt and that area is called Kittilä greenstone complex (Hanski and Huhma, 2005) or Kittilä greenstone area (Rastas et al., 2001). The Kittilä suite includes massive amount of mafic metavolcanic rocks, hyaloclast, tuffites and breccias (Hanski and Huhma, 2005). Thickness of these folded volcanic rocks reach probably vertically even 9 km based on geophysical measurements (Niiranen, 2015). There are also different types of sedimentary interbeds and larger sedimentary units. These includes metagraywackes, phyllites, graphite- and sulfite bearing schists, and minor carbonated rocks. One of the most markable of these sedimentary units are banded iron-formations (e.g. Porkonen Formation; Hanski and Huhma, 2005). Many 2.01 Ga pre-thrusting and 1.92 Ga post-thrusting granodiorite rocks is cutting the Kittilä suite rocks what give maximum deposition age ca. 2.0 Ga (Köykkä et al., 2019).

2.1.6. Kumpu group

Originally, Kumpu and former Lainio group were divided into two separate groups and are now combined to Kumpu group due to their similarities (Hanski and Huhma, 2005). The youngest rocks of the Central Lapland belt are belonging to the Kumpu group with maximum depositional age dated to be ca.1.88 Ga, determined from clast within Kumpu group conglomerates (Lehtonen et al., 1998; Hanski and Huhma, 2005). There is no reliable field evidence that the 1.80 Ga granites cut Kumpu group rocks, but they are known to cut Kittilä and Savukoski group rocks (Hanski et al., 2001)

The Kumpu group is comprised of 200-2000m thick sedimentary units. The Kumpu group rocks are the youngest arenaceous metasediments in the northern Finland (Lehtonen et al., 1998). Lithologies are coarse, molasse-like metasediments and they usually lie on folded formations of older groups. Typical feature of this group is red-brown and purple tint for rocks due to hematite pigment. Kumpu group conglomerates have clasts of rock

types from underlying formations. The clasts include mafic metavolcanic rocks, tuffites, different kinds of schists, quartzite, arkose quartzite, vein quartz, chert, iron ore, albitite, rare carbonate rock as well as magmatic rocks such as metagabbro, diabase, granitoids, and felsic porphyries and red jasper fragments. They may also include some pebbles from older conglomerates (Hanski and Huhma, 2005). The type formation of the Kumpu group is the Levi formation which is located near the village of Sirkka village. Along with Kumpu group metasediments, minor calc-alkaline volcanic rocks occurring in the CLB has also an age of ca. 1.88 Ga (Hanski et al., 2001).

3. FORMATION OF GOLD DEPOSITS AND THEIR OCCURRENCE IN CLB

Earth's crust contains average only 0.005 g of gold for each ton of rock which means gold need to enrich that it can be mineable. In nature, gold is often alloyed with silver or copper, also tellurides and selenides are common components in some systems. Gold often occurs together with pyrite and arsenopyrite (Herrington and Stanley, 2001).

3.1. Formations of gold deposits

According to Herrington and Stanley (2001) is recognized six or seven world-class primary gold deposit types excluding secondary deposits, as like placers: orogenic gold deposits, Carlin-type gold deposits, epithermal deposits, porphyry copper-gold deposits, iron oxide copper-gold deposits, gold-rich massive sulfide deposits. The seventh deposit type is Witwatersrand pebble-conglomerate type which may be an ancient alluvial placer.

Orogenic gold deposits forms during compressional to transpressional deformation processes at convergent plate margins in accretionary and collisional orogens. Subduction related thermal events, initiate and drive long-distance hydrothermal fluids migration. Gold be carried by hydrothermal fluid and forming gold-bearing quartz to mineable distance (Groves et al., 1998). Mineralogy of these deposits are usually quartz-dominant vein systems with $\leq 3-5\%$ sulfide minerals (mainly Fe-sulfides) and $\leq 5-15\%$ carbonate minerals. Albite, white mica, or chlorite, fuchsite, scheelite and tourmaline are also common gangue phases in veins in greenschist-facies host rocks (Groves et al., 1998).

Carlin-type deposits are epigenetic, disseminated, auriferous pyrite deposits enriched in As, Sb, Hg, and Tl that are typically hosted in calcareous sedimentary rocks. Deposits is named after a deposit near Carlin, Nevada. Gold ore in these deposits, usually occurs at intersections between faults and permeable reactive strata typically below an impermeable caprock and generally exhibits a central high-grade zone of carbonate

dissolution and argillic alteration with micron-sized disseminated pyrite (Saunders et al. 2014).

Epithermal deposits at depths less than about 1,500 meters below the water table, in the uppermost parts of the crust, and at temperatures below about 300 °C. Most epithermal gold-silver deposits are related genetically to hydrothermal systems which are associated subaerial volcanism and intrusion of calc-alkaline magmas along convergent plate margins. Most known epithermal deposit are Cenozoic, but these deposits formed throughout most of geologic time (John et al. 2010)

Porphyry copper deposits are important potential sources for gold in lower temperature epithermal deposits and they are among the largest reservoirs of gold in the upper crust. Gold in porphyry copper deposits is found in solid solution in Cu-Fe and Cu sulfides and as small grains of native gold, often along boundaries of bornite (Kesler and Chryssoulis, 2002) Forming porphyry copper deposits are related to magma chambers deep below the deposit. Gold concentration of porphyry copper deposit can change a lot with different kind of formations. Hydrothermal fluids are associated gold enrichment in the porphyry copper deposits. (Chiaradia, 2020).

Iron oxide copper-gold (IOCG) deposits are formed from magmatic hydrothermal fluids and have many similarities with porphyry copper deposits, although there are also important differences. IOCG deposits are Fe oxide rich and have volumetrically extensive high-temperature alteration zones. These deposits occur predominantly occur in Precambrian rocks (Richards and Mumin, 2013). Formation depth of IOCG deposits ranges from the deep the upper crust to paleosurfaces (Groves et al., 2010).

Gold-rich volcanogenic massive sulfide (Au-VMS) deposits are defined a sub-type of both volcanogenic massive sulfide (VMS) and lode gold deposits. They consist of semi-massive to massive, concordant sulfide lenses underlain by discordant stockwork feeder zones as most VMS deposits. The main difference between other VMS deposits and Au-VMS deposits is their gold concentration (Dube et al., 2007).

3.2. Gold occurrences in Central Lapland belt

In Finland, supercontinent evolution of the region between ~2.75–1.77 Ga includes all gold-mineralized environments in here, except the possible Archean epithermal deposits and the recent placers. During the main stages of crustal growth globally 2.72–2.64 Ga and 1.91–1.77 Ga was formed most of the gold deposits in Finland (Eilu, 2015). Orogenic

gold deposits are most common of the gold deposit types in Finland. One age group of orogenic gold deposits in Finland is related to the Svecofennian composite orogenies, at 1.91–1.77 Ga. During a continent–continent collision event at 1.84–1.78 Ga probably took place most of the Paleoproterozoic mineralization (Eilu, 2015).

Suurikuusikko gold deposit in Central Lapland belt, in Kittilä is the largest known gold deposit in northern Europe (Patisson et al., 2007). According to Wyche et al. (2015) Re–Os age of 1916 ± 19 Ma obtained from gold-bearing arsenopyrite suggest that Suurikuusikko mineralization took place 60–100 Ma after Kittilä group deposition and before the end of collision-related sedimentation in the CLGB. Suurikuusikko has almost all features for typical an orogenic gold deposit. (Wyche et al. 2015). Repeated reactivation of major faults with barren hydrothermal pulses occurred between 1.86–1.81 Ga in CLB. In Kittilä province gold deposition of several small deposits (e.g. Levijärvi, Iso-Kuotko, Saattopora) are overprinted by the early hydrothermal assemblages during the 1.81–1.75 Ga, late-to post-orogenic stages of the Svecofennian tectonic evolution (Molnar, 2021).

4. ZIRCONS IN GEOCHRONOLOGY AND U-Pb DATING

Zircon ($ZrSiO_4$) is highly potential for U-Pb dating due to its excellent properties. It is very hard mineral with 7.5 Mohs hardness scale and because of that, it has good resistance for mechanical weathering. Zircon has high melting temperature, and it also has good resistant to chemical weathering and metamorphism. Zircon has relatively high density (4.6 g/cm^3) and non-magnetic which makes it easier to separate using heavy liquid separation. It has measurable amount of U and usually very high $^{238}\text{U}/^{204}\text{Pb}$ ratio, meaning that zircon incorporates negligible amount of non-radiogenic lead into its crystal structure. Zircon is common accessory mineral in variety igneous and metamorphic rocks and it can survive many sedimentary cycles (Pirckle and Podmeyer, 1993), making it one of the most common geochronological tools for metasedimentary studies.

Radiation damage and hydrothermal alteration can be seen from zircons through changes in crystal structures, oxygen isotope values and petrographic and geochemical characteristics. Alteration states of zircons can be seen from their Th, U and REE contents (Liu et al., 2019). Variable morphologies and internal structures are seen in metamorphic zircons formed under different metamorphic conditions. Metamorphic zircons can have example different zoning structures (Wu and Zheng, 2004), with zones representing

different stages of zircon growth (e.g. metamorphic vs. hydrothermal; e.g. Rubatto et al., 1999).

4.1. U-Pb analyses

In nature, uranium (U) has three radioactive isotopes. Isotopes ^{238}U (~97.275%) and ^{235}U (0.720%) are the most common ones but there is also small amount of ^{234}U (~0.005%) isotope in nature (Babu et al., 2008). Isotopes ^{238}U and ^{235}U are used in geochronology. Isotope ^{238}U decays to stable ^{206}Pb but decaying is not direct but goes through series of short-lived daughter isotopes before the stable radiogenic ^{206}Pb . The isotope half-life to ^{206}Pb is 4.468 Ga. Isotope ^{235}U decays to stable ^{207}Pb By similar type of decay chain of short-lived daughter isotopes. This isotope half-life to ^{207}Pb is 703.8 Ma (Schoene, 2014).

Non-radiogenic lead isotope ^{204}Pb is called common lead in U-Pb geochronology. Common lead can cause bias to age determination. It only occurs trace amounts in zircon crystallizing but it can increase during weathering or hydrothermal alteration. The common lead can also increase from contamination of molding chase or other sample preparations chases (Andersen et al., 2019).

There are four isotopes (^{204}Pb , ^{206}Pb , ^{207}Pb , ^{208}Pb ,) for natural Pb. Three of these are radiogenic. Here are the equations for the radiogenic isotopes (Vermeesch, 2021) (Formulas 1, 2, 3):

$$^{206}\text{Pb}^* = ^{238}\text{U}(e^{\lambda_{238}t} - 1) \quad (1)$$

$$^{207}\text{Pb}^* = ^{235}\text{U}(e^{\lambda_{235}t} - 1) \quad (2)$$

$$^{208}\text{Pb}^* = ^{232}\text{Th}(e^{\lambda_{232}t} - 1) \quad (3)$$

The ingrowth equations for the three radiogenic Pb isotopes with $\lambda_{238} = 1.551359 \times 10^{-10} \text{a}^{-1}$ ($t_{1/2} = 4.468 \text{ Ga}$), $\lambda_{235} = 9.845841 \times 10^{-10} \text{a}^{-1}$ ($t_{1/2} = 703.8 \text{ Ma}$), and $\lambda_{232} = 0.4933431 \text{ P} \times 10^{-10} \text{a}^{-1}$ ($t_{1/2} = 14.05 \text{ Ga}$)

The corresponding age equations are (Vermeesch, 2021) (Formulas 4, 5, 6):

$$t_{206} = \frac{1}{\lambda_{238}} \ln \left(\frac{^{206}\text{Pb}^*}{^{238}\text{U}} + 1 \right) \quad (4)$$

$$t_{207} = \frac{1}{\lambda_{235}} \ln \left(\frac{^{207}\text{Pb}^*}{^{235}\text{U}} + 1 \right) \quad (5)$$

$$t_{208} = \frac{1}{\lambda_{232}} \ln \left(\frac{^{208}\text{Pb}^*}{^{232}\text{U}} + 1 \right) \quad (6)$$

The equation for normalizing common lead (^{204}Pb) (Vermeesch, 2021) (Formulas 7, 8, 9):

$$\frac{^{206}\text{Pb}}{^{204}\text{Pb}} = \left(\frac{^{206}\text{Pb}}{^{204}\text{Pb}}\right)_0 + \frac{^{238}\text{U}}{^{204}\text{Pb}} (e^{\lambda_{238}t} - 1) \quad (7)$$

$$\frac{^{207}\text{Pb}}{^{204}\text{Pb}} = \left(\frac{^{207}\text{Pb}}{^{204}\text{Pb}}\right)_0 + \frac{^{235}\text{U}}{^{204}\text{Pb}} (e^{\lambda_{235}t} - 1) \quad (8)$$

$$\frac{^{208}\text{Pb}}{^{204}\text{Pb}} = \left(\frac{^{208}\text{Pb}}{^{204}\text{Pb}}\right)_0 + \frac{^{232}\text{Th}}{^{204}\text{Pb}} (e^{\lambda_{232}t} - 1) \quad (9)$$

Because different isotopes have same parent-daughter pair, U-Pb datings have access to two separate geochronometers ($^{206}\text{Pb}/^{238}\text{U}$ and $^{207}\text{Pb}/^{235}\text{U}$) that can be evaluated separately and together. This makes U-Pb dating reliable technique and powerful tool in geochronology (Vermeesch, 2021)

$^{206}\text{Pb}/^{238}\text{U}$ and $^{207}\text{Pb}/^{235}\text{U}$ are presented together in so-called concordia diagram by Wetherill (1956). Concordia curve is not linear due to the different half-lives of the ^{238}U and ^{235}U isotopes. If mineral under dating has remained as close system after its crystallization, sample will plot on the concordia curve and age can be determined directly. If mineral system has been opened at some point of the history after crystallization, it could have lost e.g. part of the radiogenic lead. Therefore, the sample do not plot directly on to the concordia curve, but below or in top of it and sample is said to have discordant age (Schoene, 2014). Discordant arrays can be caused by Pb loss, Pb gain, U loss, U gain and mixing of different-aged material. Usually, in a sample, there are several data points with similar evolution but with different amounts of Pb loss. This difference can form linear path from the origin towards the date which corresponds the real age on concordia curve (Figure 3a). This line can also cut the concordia curve at above origin and the cutting point corresponds to the time of the Pb-loss event. The upper cutting point can then correspond the true formation age of the mineral (Figure 3b). This method can give valuable information from Pb-loss events and give new tools to interpret datings (Schoene, 2014).

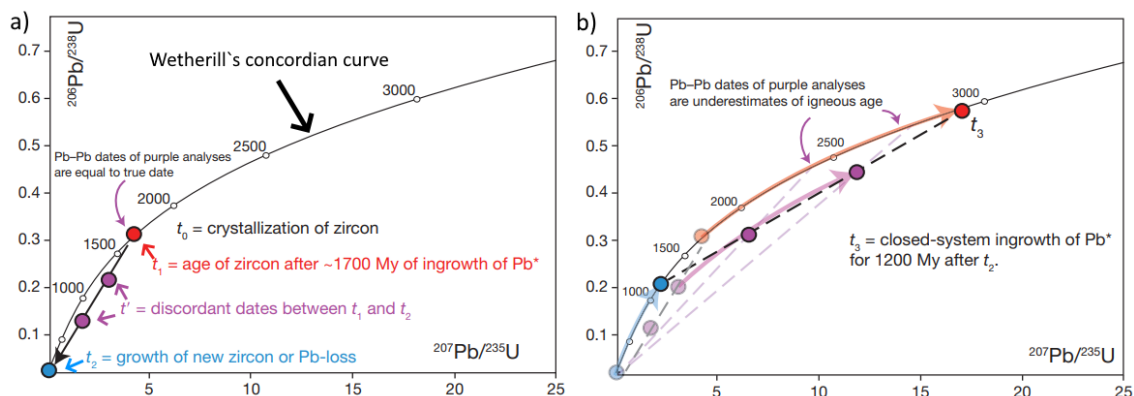


Figure 3. Pb-loss event present on Wetherill's concordia curve (Modified from Schoene, 2014).

4.2. Metamorphic zircons and alteration of zircons

According to Williams (2001), zircon is suggested being relatively refractory during low- to moderate-pressure metamorphism, but recent studies have suggested that it is possible for zircon also to alter in relatively low temperatures. Spandler et al., (2004), reported one of the lowest temperatures of zircon alteration in metamorphic rocks where temperature was <100 °C. More common alteration and metamorphic growing is observed in temperatures 250-450 °C (Kohn et al., 2018). Kohn et al., (2018), represented four different ways to form metamorphic zircon: low-grade processes (Figure 4a), retrograde release of Zr from major minerals (Figure 4b), crystallization of in situ melts (Figure 4c), and Ostwald ripening (Figure 4d).

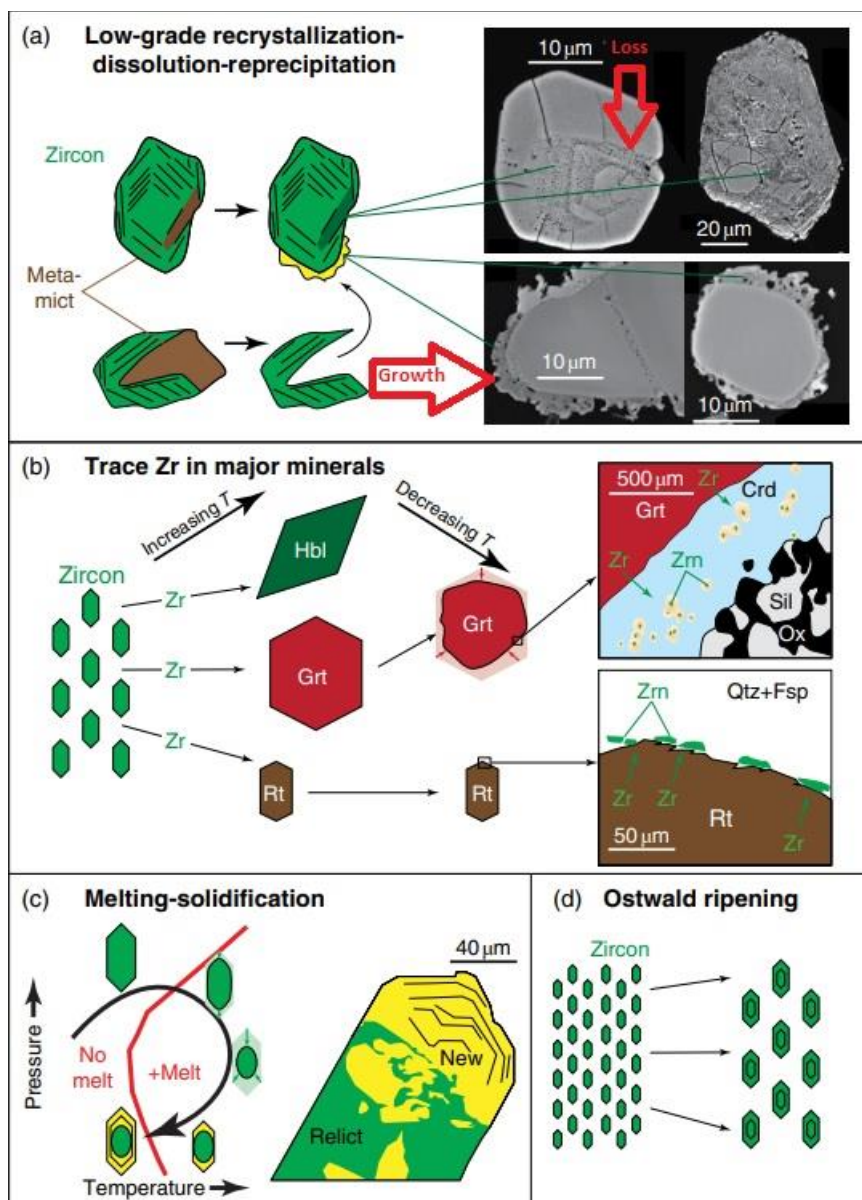


Figure 4. Four different ways to form metamorphic zircons. Modified figure from Kohn et al., (2018).

Alpha radiation is the most important cause as zircon becoming to metamictic state. Zircon can change to amorphous during metamictization (Nasdala et al., 1996). In low-grade processes metamict zircon may dissolve or recrystallize and reprecipitate either within a crystal or as overgrowths on other crystals (Figure 4a) (Kohn et al., 2018).

Zr concentrations of most silicates are extremely low. Few minerals, especially garnet, hornblende and rutile can contain ppm-level concentration of Zr and the concentration increases exponentially when temperature increases. Typical rocks contain approximately 100-200 ppm Zr dominantly is hosted in zircon at low metamorphic grades. Rocks with

rutile, garnet or hornblende can contain a lot more Zr (Kohn et al., 2018). Several percent of zircon must dissolve that Zr can provide to rutile, garnet and hornblende. As temperature increases, zircon dissolves and rutile, garnet and hornblende must first grow that they can take up increasingly more Zr (Figure 4b). Figure 4c present a zircon grain which is reform during cooling. Melt has formed younger overgrowths on rim of older zircon nuclei. Textures of zircons in migmatitic rocks support this assumption. In paleosomes, zircons occur usually rounded and do not display zircon overgrowth around the cores that have not interacted with melts. In contrast, zircons in leucosomes or in melanosomes that have interacted with melt, exhibit euhedral shapes and can have large late-stage overgrowths (Kohn et al., 2018).

Ostwald ripening is a thermodynamically driven process. It is due to a larger crystal having less surface-free energy relative to total free energy than a smaller crystal. Smaller crystals dissolves and larger crystals grows because of that difference in free energy. When small crystals become smaller their dissolution rates should accelerate (Figure 4d) (Kohn et al., 2018).

Zircon alteration is usually caused by re-equilibration, recrystallization, dissolution-reprecipitation, neoblastic growth, and/or metamictization. Characteristic to zircon alteration are structural, isotopic and geochemical changes to the original crystal which usually exhibited as distinct micrometer to submicrometer mineral domains (Schneider et al., 2012). Often alteration zones of zircon have overlooked and removed for conventional U-Pb geochronology due to that they disturb normally concordant isotopic systems. It has been studied that chemical and isotopic systems of the alteration zones have signatures in which can obtain valuable geological information from the timing and nature of fluid influx (Schneider et al., 2012). According to Lankvelt et al., (2016), under lower temperature conditions, hydrothermally precipitated and altered precipitated zircon may be associated with metallic ore deposits.

4.3. Use of sedimentary rocks and detrital zircons in age dating

Detrital zircons occur in almost every sedimentary rock. Sedimentary rocks could contain zircons from many different sources (Tapia-Fernandez et al., 2017). Detrital zircons end up to sedimentary rocks by first eroding from pre-existing rocks and then transporting during sedimentation. Finally, they are part of sedimentary rocks (Morton and Hallsworth, 1999). Detrital zircons record important information from their origin

(Condie et al., 2009). One study from Australia shows, that the youngest detrital zircons in Holocene beach sands are Permian making them 250 Ma older than the age of deposition (Tapia-Fernandez et al., 2017). This example explains that detrital zircons in sedimentary rock can be much older than the actual sedimentation age.

Since at least 3.7-3.8 billion years ago, sediments have been continuously deposited. Sediment rocks are most common lithology in the geological record. Sedimentary rocks record important information from geological and biological events. Among other things, the information obtained from the geochronology can show scale and duration of events (Rasmussen, 2005). Publications from detrital zircon geochronology are exponentially increased in the 2000s. This is due to that technical advance have made it possible to efficiently determine reliable U-Pb ages from individual crystals (Gehrels, 2014).

Maximum depositional age of the sedimentary units can be determined from youngest detrital zircon grain because sedimentary unit cannot be older than its youngest zircons. There are still several things what can affect age results, for an example Pb loss which increases the analytical uncertainties (e.g., Gehrels, 2014). That means that the results usually have both younger and older ages than the true age of the unit. Most cases the youngest age will be younger than the true age (Gehrels, 2014). Method to avoid this problem, is to use the age of the youngest group of ages from sample (Dickinson and Gehrels, 2009). One of these methods is $YC1\sigma(2+)$ what is defined by sorting all analyses by their U-Pb age plus 1σ uncertainty and identifying the youngest cluster of 2 or more ages of analyses with overlapping 1σ error (Sharman et al., 2018).

Despite these uncertainties, the youngest detrital zircon grains often give useful information about depositional age (Gehrels, 2014). Gehrels (2014) presented several studies which have used detrital zircons of sedimentary rocks for many different purposes. One example of that is a study of early earth evolution with detrital zircons. (Harrison, 2009). In future there are many possibilities for detrital zircon research when new analytical methods and applications are developed (Gehrels, 2014).

4.4. Morphology of zircon grains

Roundness of zircon grains and their ages can be used to study their physical transportation processes (Pupin, 1980). Morphology of the crystals can potentially reveal information of the zircons transportation, deposition and recycling processes of the sedimentary environment. Detrital zircon grains that have undergone extreme alluvial or

olian processes and have recycled multiple times, are usually highly rounded. Zircon grains which have undergone limited transport can imply more angular (Köykkä et al., 2019).

5. SAMPLING AND ANALYTICAL METHODS

5.1. Sampling

Samples for the age determination were collected from drill cores owned by Rupert Finland Oy. 10 representative $\frac{1}{4}$ core samples were collected with total weight approximately 223 kg.

Geology survey of Finland (GTK) conducted the sample preparation, analyzing and helped with data processing. Handpicking of the zircon grains and SEM-BSE imaging was done in the Geological Survey of Finland Laboratory in Espoo.

5.2. Sample preparation

Approximately 5 kg per sample were crushed with cone crusher. Crushed samples were sieved to 7 different fractions from largest to smallest >2 mm, 2-1 mm, 1 mm-500 μm , 500-250 μm , 250-125 μm , 125-63 μm and <63 μm . Fraction 125-63 μm was used to heavy liquid separation (diiodomethane, $d= 3.325 \text{ kg/m}^3$). Zircon have density about 4.7 kg/m^3 so zircon along with other heavy mineral grains sink to bottom of the sample container. 9 of 10 from samples have left more than 0.05g heavy fraction after separation. Only from a 120112-A sample resulted no heavy fraction at all from 125-63 μm fraction. New heavy liquid separation with 250-125 μm fraction was done to that sample and resulted more than 0.05g heavy fraction left. Zircon grains were handpicked under the microscope. The goal was to pick at least 100 zircon grains in order to get statistically meaningful age distribution from dating.

5.3. LA-ICPMS Attom

Zircon grains for U-Pb dating were selected by hand-picking from the delivered fractions, after additional separation steps (sulphide removal, clerici separation). The grains were mounted in epoxy resin and sectioned approximately in half and polished. Back-scattered electron images (BSE) and cathodoluminescence (CL) images were prepared for the zircons to target the spot analysis sites. U-Pb dating analyses were performed using a Nu Plasma AttoM single collector ICPMS at the Geological Survey of Finland in Espoo connected to a Photon Machine Excite laser ablation system. Samples were ablated in He gas (gas flows in mass flow controllers = 0.4 and 0.1 l/min) within a HelEx ablation cell

(Müller et al., 2009). The He aerosol was mixed with Ar (gas flow= 0.98-0.99 l/min) prior to entry into the plasma. The gas mixture was optimized daily for maximum sensitivity. Ablation conditions were: beam diameter: 20 μm , pulse frequency: 5 Hz, beam energy density: 2.17 J/cm². A single U–Pb measurement included a short pre-ablation with a 25 μm beam, 10 s of on-mass background measurement, followed by 30 s of ablation with a stationary beam. ²³⁵U was calculated from the signal at mass 238 using a natural ²³⁸U/²³⁵U=137.88. Mass number 204 was used as a monitor for common ²⁰⁴Pb. The contribution of ²⁰⁴Hg from the plasma was eliminated by on-mass background measurement prior to each analysis. Age related common lead (Stacey and Kramers, 1975) correction was used when the analysis showed common lead contents significantly above the detection limit (i.e., >60 cps). Signal strengths on mass 206 were typically 250000 cps, depending on the uranium content and age of the zircon.

Calibration standard GJ-1 (609 \pm 1 Ma; Belousova et al., 2006), in-house reference samples A382 (1877 \pm 2 Ma, Huhma et al, 2012), and A1772 (2712 \pm 2 Ma, Huhma et al., 2012) were run at the beginning and end of each analytical session, and at regular intervals during sessions. Raw data were corrected for the background, laser induced elemental fractionation, mass discrimination and drift in ion counter gains and reduced to U–Pb isotope ratios by calibration to concordant reference zircons, using the program Glitter (Van Achterbergh et al, 2001). Further data reduction including common lead correction and error propagation was performed using excel spreadsheet written by Y. Lahaye and H. O'Brien. Errors include measured within-run errors (SD) and quadratic addition of reproducibility of standard (SE). Estimated errors in the calibration standard GJ1 were: 0.2% for ²⁰⁷Pb/²⁰⁶Pb, and 2% for both ²⁰⁶Pb/²³⁸U and ²⁰⁷Pb/²³⁵U. To minimize the effects of laser-induced elemental fractionation, the depth-to-diameter ratio of the ablation pit was kept low, and isotopically homogeneous segments of the time-resolved traces were calibrated against the corresponding time interval for each mass in the reference zircon. Plotting of the U-Pb isotopic data and age calculations were performed using the Isoplot/Ex 3 program (Ludwig, 2003). All the ages were calculated with 2 σ errors and without decay constants errors. Data-point error ellipses in the figures are at the 2 σ level. The ²⁰⁷Pb/²⁰⁶Pb age offset from concordant ID-TIMS ages for several samples does not exceed 0.5%.²

6. RESULTS

Samples in this study represent conglomerates and variable altered quartzites. Individual samples and their lithologies are listed in the Table 1.

Table 1. Sample Id, hole Id and lithologies of the samples.

Sample Id	Hole Id	Lithology
120059_A	120059	Conglomerate
120063_A	120063	Sericite-albite altered quartzite
120071_A	120071	Conglomerate
120074B_A	120074B	Sericite altered quartzite
120094&120097_A	120094&120097(Combined)	Sericite altered quartzite
120098_A	120098	Sericite altered quartzite
120100_A	120100	Sericite-albite altered quartzite
120112_A	120112	Sericite altered quartzite
120112_B	120112	Sericite-albite altered quartzite
120112_C	120112	Sericite-albite altered quartzite

6.1. Petrographic description

Conglomerates

120059_A is conglomerate located within the central part of the Ikkari deposit. The thin section is comprised of quartz (80%), biotite (10%), carbonates (6%) and opaque (4%) as primary minerals and chlorite and zircon as accessory minerals. The conglomerate is matrix-supported. Matrix of thin section varies a lot (Figure 5a). There are mainly coarse undulating quartz clasts with fine grained quartz, carbonate grains and quite lot of large opaque minerals. There are also one large and several smaller spots of biotite. Biotite is locally showing alteration to chlorite. Opaque minerals are pyrite and magnetite.

120071_A is conglomerate within central part of the Ikkari deposit. The conglomerate is matrix-supported. Matrix is very fine sericite and quartz (Figure 5c). The thin section has medium clastic texture. Clasts are composed of quartz. The thin section has quartz 75%, sericite 18%, plagioclase/albite 5% and carbonate 2% as primary minerals and as accessory minerals are zircon and opaque which are mainly pyrite and magnetite.

Quartzites

The sample 120074B_A is sericite altered quartzite within the central part of the Ikkari deposit. There are mostly coarse quartz grains in sericite-quartz matrix. Also there occurs fine grained quartz veins. The thin section has fine clastic texture. At least one chlorite vein is in this thin section (Figure 5d). All opaque minerals are in chlorite vein in this thin section and those are mainly magnetite. The thin section has quartz 70%, sericite 20%, chlorite 9% and opaque 1% as primary minerals and zircon and carbonates as accessory minerals.

120094&120097_A is sericite altered quartzite within the central of the Ikkari deposit. Coarse quartz grains occur in fine grainsized sericite matrix (Figure 5e). Middle of the thin section occur 2mm wide carbonate vein with plenty of opaque minerals. Opaque minerals are mainly magnetite and pyrite. The thin section has quartz 60%, sericite 25%, carbonates 12% and opaque 3% as primary minerals and k-feldspar, plagioclase/albite, biotite, chlorite, and zircon as accessory minerals.

The sample 120098_A is sericite altered quartzite within northern the Ikkari deposit. Thin section has quartz 85%, sericite 10% and opaque 5% as primary minerals. Carbonates and zircon occur as accessory minerals. Coarse quartz grains occur in very fine grainsized sericite matrix (Figure 5f). The thin section has medium clastic texture. Opaque minerals, mostly magnetite grains, occur all over thin section. Hematite inclusions occur in magnetite grains.

The sample 120112_A is sericite altered quartzite within northern part of Ikkari deposit. The thin section has quartz 45%, sericite 35%, carbonates 15% and opaque 5% as primary minerals and zircon as an accessory mineral. Base matrix is very fine grainsized quartz-sericite mix with fine hematite grains (Figure 6b). There are two coarse grainsized carbonates-quartz veins parallel to orientation of base matrix. In those carbonate-quartz veins occur a bit of gold (Figures 9c & 9d). Micro folding/crenulation cleavage can be seen from sericite-quartz matrix.

The sample 120063A represents sericite-albite altered quartzite located in the western part of the Ikkari deposit. Coarse quartz grains occur in very fine-grained sericite and quartz matrix (Figure 5b). There also are also some quartz veins where grainsize is coarse grained. Sericite-quartz matrix is lightly foliated. The thin section has quartz 70%, sericite

20%, albite 7%, carbonate 2% and opaque 1% as primary minerals and biotite and zircon as accessory mineral. Opaque minerals are mainly magnetite.

The sample 120100 A is sericite-albite altered quartzite sample within central of the Ikkari deposit. The thin section has quartz 50%, carbonate 20%, sericite 16%, plagioclase/albite 10% and opaque 4% as primary minerals and as an accessory mineral it has zircon. Matrix is fine quartz and albite grains in very fine sericite matrix (Figure 6a). There is large calcite vein in the middle of the thin section where occur a lot of opaque minerals. Opaque minerals are pyrite and magnetite.

120112 B is sericite-albite altered quartzite within northern part of the Ikkari deposit. The thin section has quartz 60%, sericite 25%, carbonates 10%, plagioclase/albite 3% and opaque 2% as an accessory mineral occur zircon. The thin section has medium clastic texture. Matrix is fine-grained sericite-quartz where are coarse quartz grains (Figure 6e). There are spots where occur carbonate grains. There are also few plagioclase/albite grains in matrix. Opaque minerals are hematite and magnetite.

The sample 120112 C is sericite-albite altered quartzite within northern part of the Ikkari deposit. The thin section has quartz 65%, sericite 15%, carbonates 10%, plagioclase/albite 7% and opaque 3% as primary minerals and zircon as an accessory mineral. Matrix is very fine grain sized sericite-quartz with many coarse grainsized quartz grains and some albite grains (Figure 6f). One 4mm wide carbonate vein occur in central part of the thin section. There are also small opaque grains allover of the base matrix. Opaque minerals are mainly magnetite with hematite exsolutions.

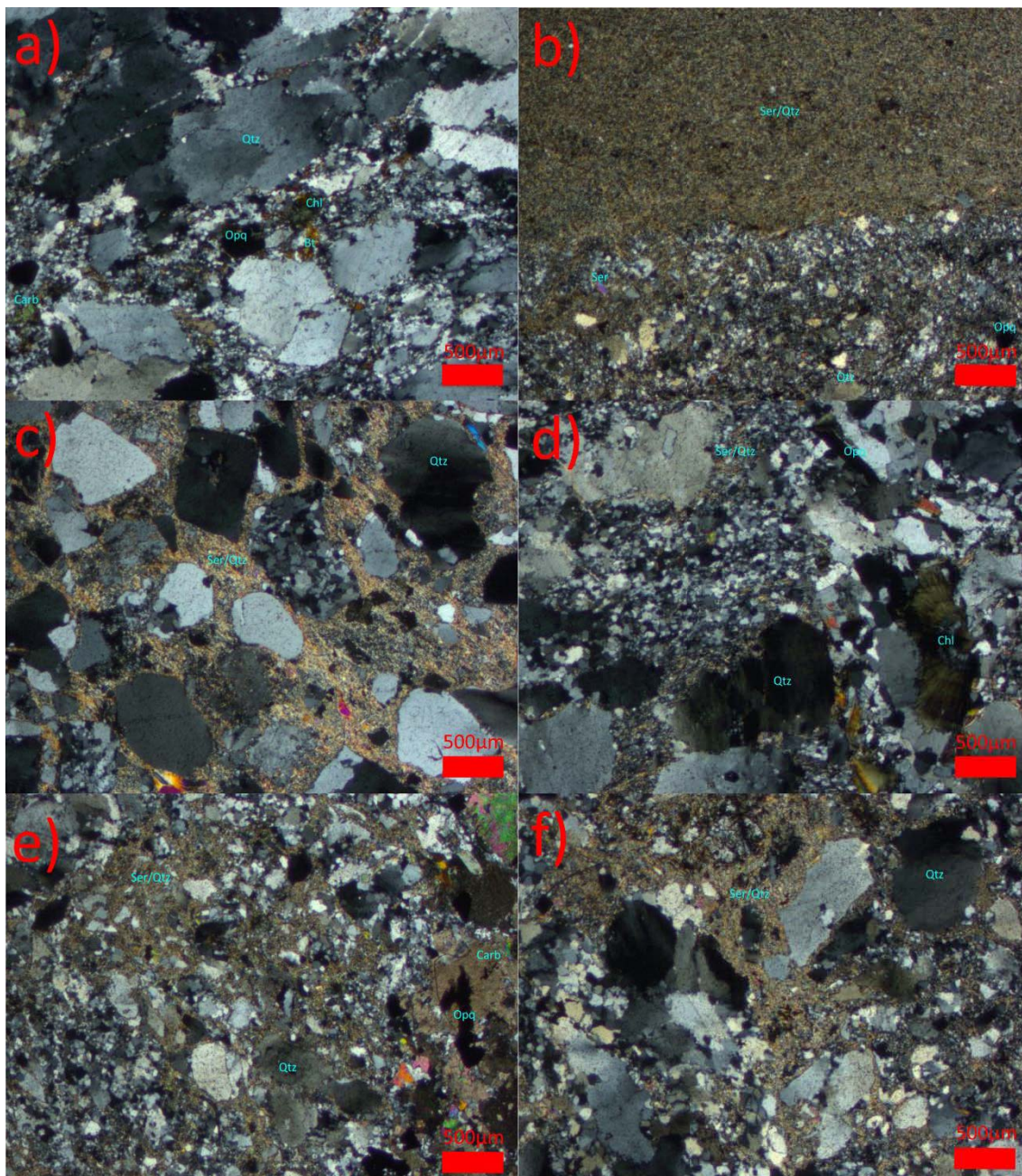


Figure 5. Thin section photomicrographs in crosses polarized light: a) 120059_A Coarse quartz clasts in finer quartz matrix; b) 120063_A. Very fine grained sericite-quartz matrix contact to fine grained sericite-quartz matrix; c) 120071_A. Coarse quartz clasts in very fine grained sericite matrix; d) 120074B_A. Coarse quartz grains in fine grained sericite-quartz matrix and chlorite vein with magnetite; e) 120094&120097_A. Coarse quartz grains in fine grained sericite-quartz matrix and carbonate vein with magnetite and pyrite; f) 120098_A. Coarse quartz grains in very fine grained sericite matrix. Bt: Biotite, Carb: Carbonate, Chl: Chlorite, Opq: Opaque, Qtz: Quartz, Ser: Sericite.

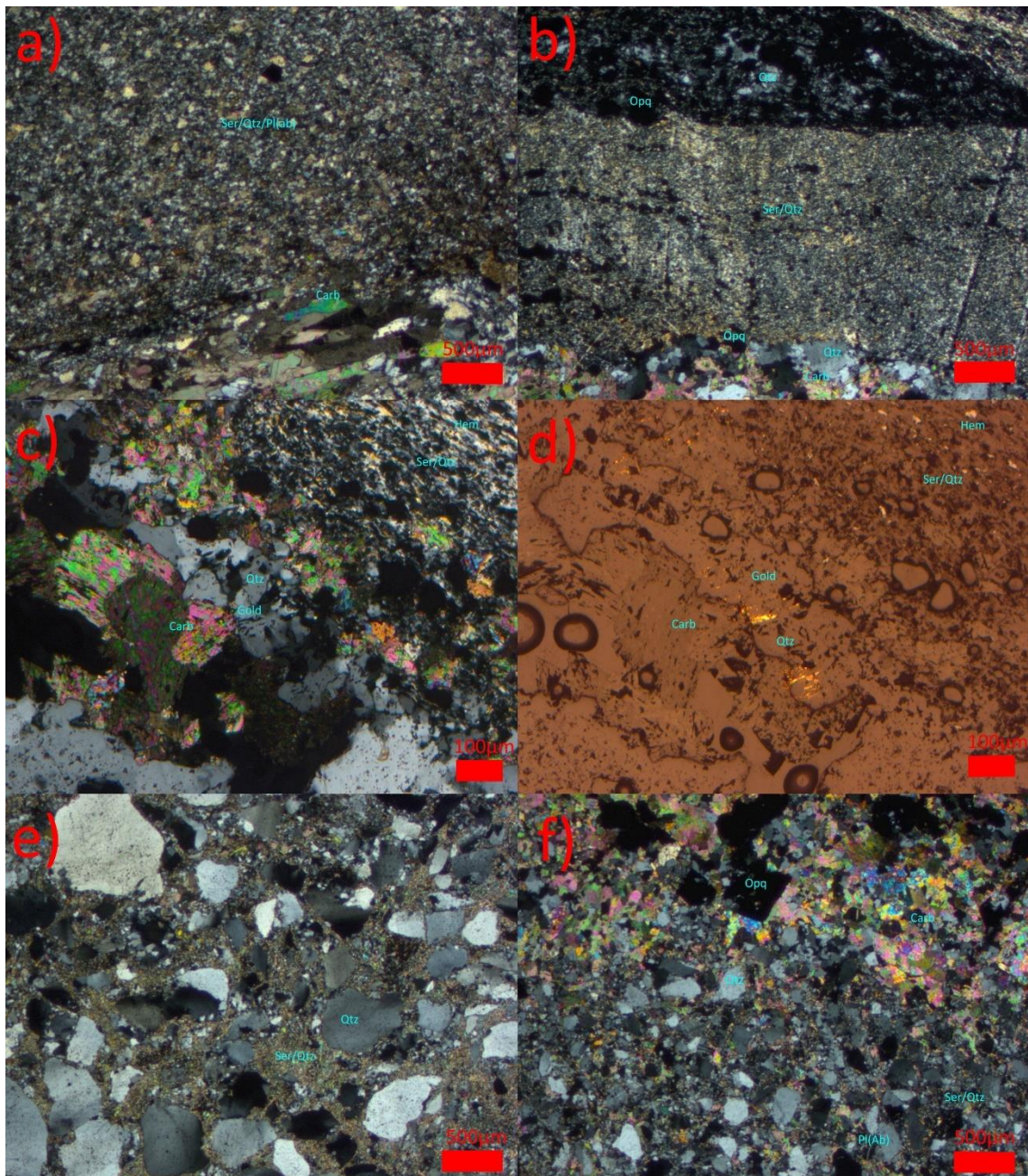


Figure 6. Thin section photomicrographs in crosses polarized light except Figure 9d in reflected light: a) 120100_A. Fine grained sericite-quartz-albite matrix and carbonate vein; b) 120112_A. Very fine grained sericite-quartz matrix between two carbonate-quartz vein; c) and d) 120112_A. Gold in quartz-carbonate vein. Fine hematite grains in sericite-quartz matrix; e) 120112_B. Coarse quartz grains in very fine grained sericite-quartz matrix; f) 120112_C Fine quartz and plagioclase (albite) grains in very fine grained sericite-quartz matrix and carbonate vein with opaque grains. Carb: Carbonate, Hem: Hematite, Opq: Opaque, Pl(ab): Plagioclase(albite), Qtz: Quartz, Ser: Sericite

6.2. U-Pb dating

Isoplot program (Ludwig, 2003) was used for data processing and age calculations. The age histograms were made for Probability Density Plot - function of Isoplot program. The plot included only concordant $^{207}\text{Pb}/^{206}\text{Pb}$ ages and their errors between 95-105% concordant-%. Analyses with high common lead content and points which contain too many inclusions were deleted. The pikes of histograms are indicating the most likely age clusters of the samples. SEM-images were taken from every zircon grain and from those images morphology of each zircon grain can be studied.

120059_A

The sample is representing conglomerate unit located within the central part of the Ikkari deposit. Detrital zircon grains are mostly subrounded or rounded and subhedral (Appendix 2). Totally 105 zircon grains were analyzed of which 19 were excluded from the age calculations due to a high common lead content or other errors. A major age population of the sample is Proterozoic and occur ca. 2015 Ma (Figure 7). The youngest age population of the sample is ca. 1910 Ma. A minor Archean age population occur ca. 2730 Ma. The sample has 24% Archean ages varying between 2500-2959 Ma and 76% Proterozoic ages varying between 1895-2484 Ma (Figure 8). Maximum deposition age of the sample is 1910 ± 10 based on the $\text{YC}1\sigma$ (2+) method (Appendix 1). Concordia diagram of the sample is presented on figure 9.

120063_A

In this quartzite sample within western of the Ikkari deposit, zircon occurs mostly rounded and anhedral grains (Appendix 2). From total 102 analyzed zircon grains 17 were excluded from results because of a high common lead content or other bias. Ca.1920 Ma occurs major population of the sample (Figure 7). The youngest reliable age population of the sample occurs ca.1876 Ma. The second largest population of the sample occurs around 2010 Ma. Also, a minor Archean population occurs around 2700 Ma. The sample has 24 % Archean ages varying between 2580-3311 Ma and 76% Proterozoic ages varying between 1842-2481 Ma (Figure 8). Sample has the youngest single age (1842 Ma) from all samples in this study. Maximum deposit age of the sample is 1847 ± 5 Ma based on $\text{YC}1\sigma$ (2+) method (Appendix 1). Concordia diagram of the sample is presented on Figure 9.

120071_A

In the conglomerate sample within central part of the Ikkari deposit zircon grains are mostly subrounded and partly euhedral (Appendix 2). Totally 101 zircon grains were analyzed of which 12 grains showed a high common lead content or other bias and were therefore excluded from the age calculations. The major age population in the sample is dated to ca. 2015 Ma (Figure 7). Also two minor populations occur close to that date, a younger around 1940 Ma and the older around 2120 Ma. A minor Archean population occur around 2730 Ma. 72% of ages of the sample are Proterozoic varying between 1913-2490 Ma and rest of the ages are Archean varying between 2694-3585 Ma (Figure 8). This sample has the oldest single age (3585 Ma) from all ages of this study. Maximum deposit age of this sample is 1919 ± 5 Ma based on YC1 σ (2+) method (Appendix 1). Concordia diagram of the sample is presented on Figure 9.

120074B_A

The sample is representing quartzite unit located within the central part of the Ikkari deposit. Zircon grains are mostly rounded or subrounded and anhedral (Appendix 2). A total of 106 grains were analyzed, but because 16 grains contained excess common lead or other errors, 90 grains were taken into account in the age calculations. The major population of sample occur around 1945 Ma (Figure 7). Only two other notable populations occur in the sample, around 2100 Ma and an Archean population around 2750 Ma. In the sample occur only 11% Archean ages varying between 2515-3051 Ma and rest 89% are Proterozoic ages varying between 1881-2336 Ma (Figure 8). Maximum deposit age of this sample is 1894 ± 7 Ma based on YC1 σ (2+) method (Appendix 1). Concordian diagram of the sample is presented on Figure 9.

120094&120097_A

Almost all zircon grains in the quartzite sample within the central of the Ikkari deposit are rounded or subrounded and most of them are anhedral (Appendix 2). 11 zircon grains from total of 106 grains were excluded due to high common lead content or other bias. Around 1930 Ma occur major population of the sample (Figure 7). Two minor populations occur around 1880 Ma and around 2000 Ma. A minor Archean population occur around 2770 Ma. The sample has 15% Archean ages varying between 2563-3108 Ma and 85% Proterozoic ages varying between 1862-2473Ma (Figure 8). Based on YC1 σ (2+) method, maximum deposition age is 1868 ± 4 Ma (Appendix 1). Concordia diagram of the sample is presented on Figure 9.

120098_A

Zircon grains in the quartzite sample within northern part of the Ikkari deposit are mostly rounded or subrounded and subhedral (Appendix 2). Totally 107 zircon grains were analyzed of which 27 grains showed a high common lead content or other errors and were excluded from the age calculations. The major populations of sample are Proterozoic and occur around 1905 Ma and 1995 Ma (Figure 7). The minor populations occur around 2110 Ma and an Archean around 2670 Ma. The Proterozoic ages vary between 1886-2367 Ma formed 87% of all ages of the sample and rest 13% are Archean ages which vary between 2553-3230 Ma (Figure 8). Maximum deposition age of the sample is 1896 ± 3 Ma based on $YC1\sigma$ (2+) method (Appendix 1). Concordia diagram of the sample is presented on Figure 10.

120100_A

Most zircon grains of the quartzite sample within central of the Ikkari deposit are subrounded and subhedral (Appendix 2). A total of 110 grains were analyzed, and because 21 grains contained excess common lead or have other errors, 89 grains were considered in the age calculations. In the sample the major population occur around 1920 Ma (Figure 7). A minor Proterozoic population occur around 2020 Ma and two minor Archean populations occur around 2535 Ma and 2735 Ma. 20% of the ages are Archean varying between 2532-3302 Ma and 80% are Proterozoic varying between 1853-2488 Ma (Figure 8). Maximum deposition age of this sample is 1860 ± 4 Ma based on $YC1\sigma$ (2+) method (Appendix 1). Concordia diagram of the sample is presented on Figure 10.

120112_B

The quartzite sample within northern part of the Ikkari deposit contain mostly rounded or subrounded and anhedral zircon grains (Appendix 2). Totally 101 zircon grains were analyzed of which 25 grains showed a high common lead content or other errors and were excluded from the age calculations. The major population of the sample occur around 1910 Ma and the only other notable population in the sample occur 2030 Ma (Figure 7). The Proterozoic ages varying 1874-2383 Ma formed 88 % of all ages and rest 12 % are Archean varying between 2602-3258 Ma (Figure 8). 1875 ± 6 Ma is inferred maximum deposition age of the sample, based on $YC1\sigma$ (2+) method (Appendix 1). Concordia diagram of the sample is presented on Figure 10.

120112_C

The most zircon grains of the quartzite sample within northern part of the Ikkari deposit are rounded or subrounded and anhedral (Appendix 2). 24 zircon grains from total of 100 grains were excluded due to high common lead content or other bias. The major population of this sample occur around 1920 Ma (Figure 7). Three minor older Proterozoic populations occur around 1995 Ma, 2050 Ma and 2100 Ma. There also occur an Archean population around 2765 Ma. 17% of the ages are Archean varying between 2619-3254 Ma and rest 83 % are Proterozoic varying between 1850-2455 Ma (Figure 8). Maximum deposition age of this sample is 1885 ± 5 Ma based on $YC1\sigma$ (2+) method (Appendix 1). Concordia diagram of the sample is presented on Figure 10.

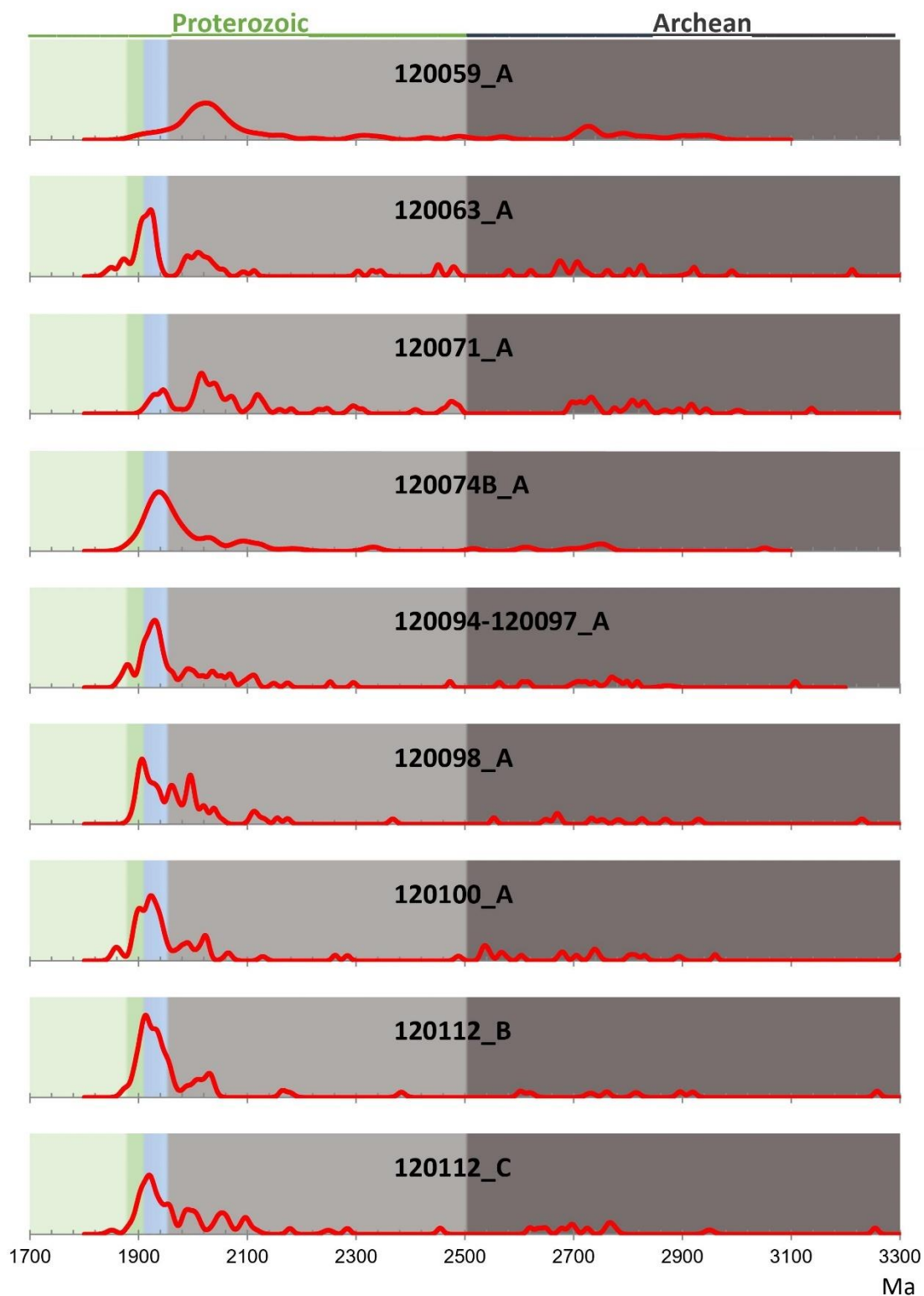


Figure 7. Probability density plots of detrital zircon $^{206}\text{Pb}/^{207}\text{Pb}$ ages of samples. Zircon grains with $< 10\%$ central discordancy were accepted for the probability density diagrams. Relative probability on the y-axis is 0-0.015. Relative probability is higher when there are more other age points close to the age. On the x-axis is timeframe from

1700 to 3300 Ma. Colors of the graphs represent times < 1.88, 1.88–1.91, 1.91–1.96, 1.96–2.50, and > 2.50 Ga from left to right.

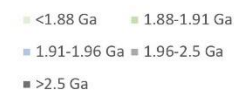
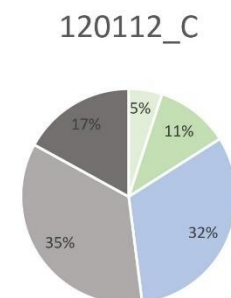
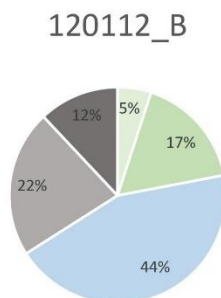
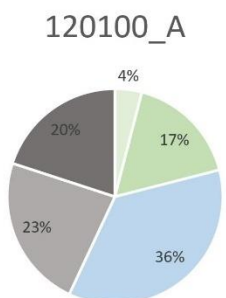
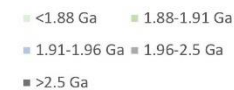
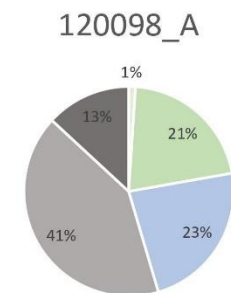
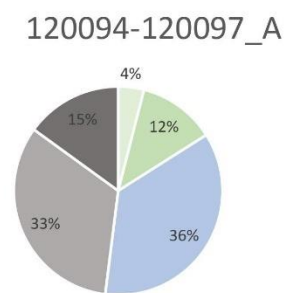
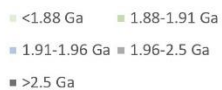
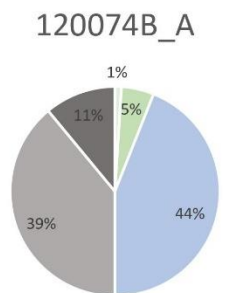
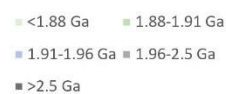
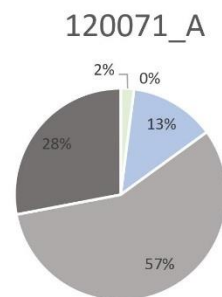
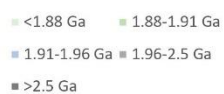
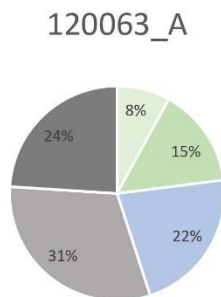
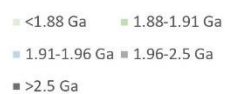
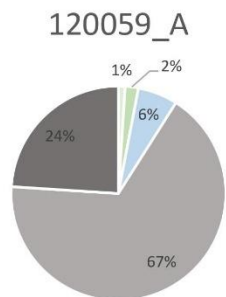


Figure 8. Pie charts represents age group distribution of the analytical results in %, which are divided into < 1.88, 1.88–1.91, 1.91–1.96, 1.96–2.50, and > 2.50 Ga.

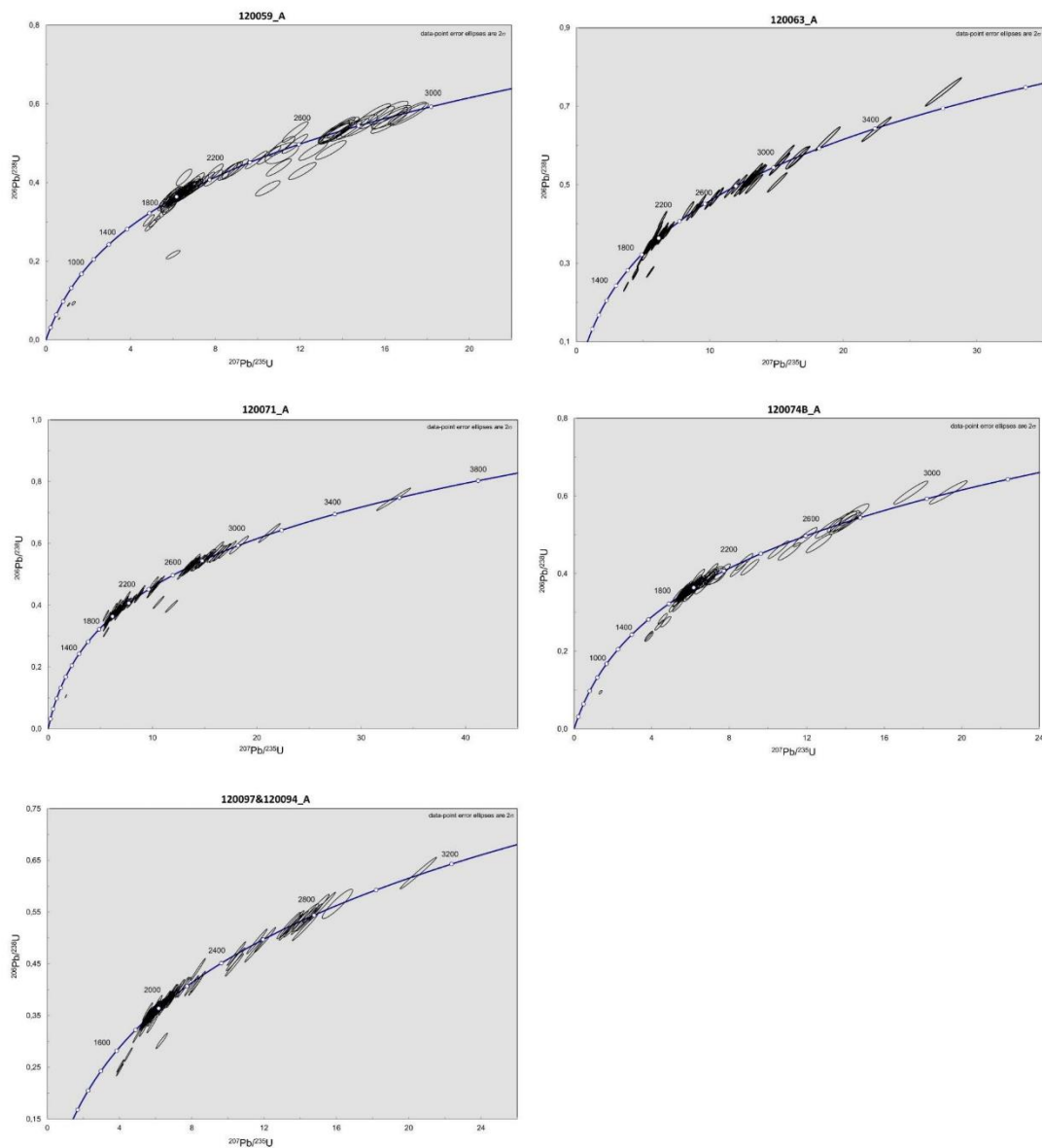


Figure 9. U-Pb concordia diagrams showing dating results with error ellipses of the analyses. Larger ellipses correspond to larger error or smaller probability density.

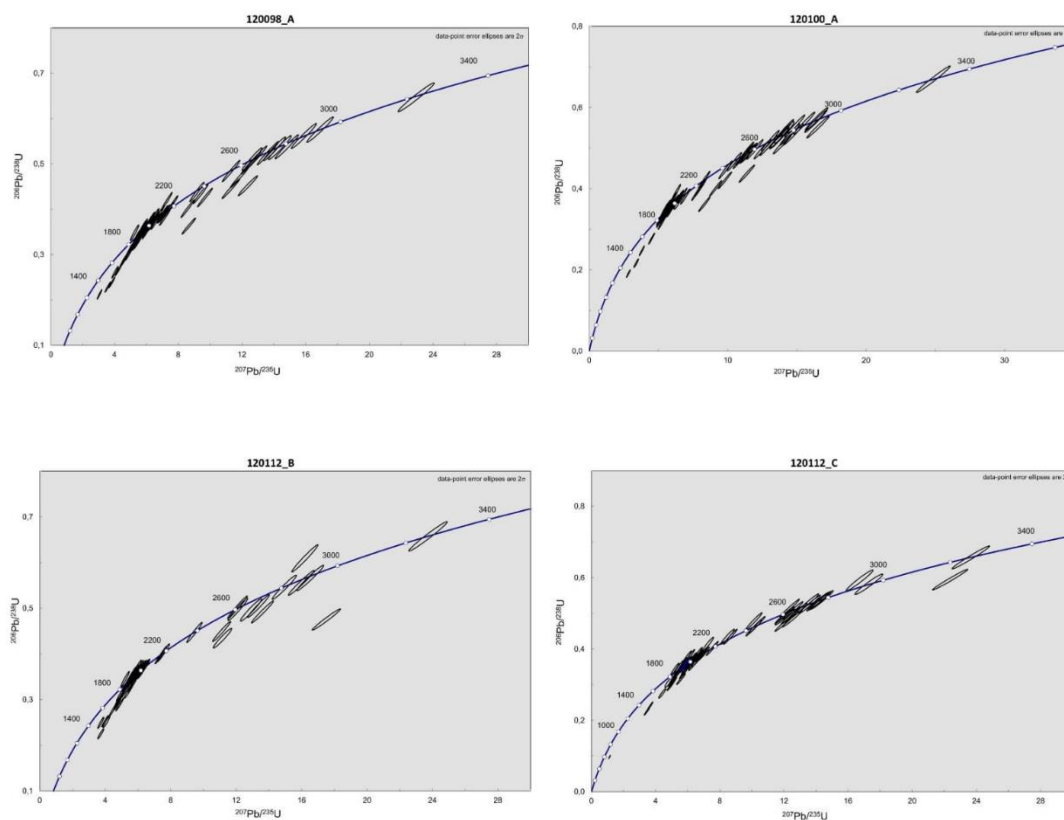


Figure 10. U-Pb concordia diagrams showing dating results with error ellipses of the analyses. Larger ellipses correspond to larger error or smaller probability density.

7. DISCUSSION

The true deposition age of the sedimentary rocks is challenging to determine due to the variable material sources and lack of high temperature processes which would produce suitable primary minerals for geochronological studies, as is the case in the magmatic or metamorphic rocks. Thus, we can only infer indirect evidences of timing of the deposition, collected from detrital mineral grains, such as zircons. Maximum age determination of the sedimentation based on the youngest zircon populations in the sediments, is commonly used (e.g. Köykkä et al, 2019). Determination of the maximum age is not always straightforward as zircon radiogenic system is often opened at some point of its history and lead to partial lead loss, and therefore they can seem younger than what they really are. If analytical errors are large, these zircons which lose lead can remain to concordia diagram. Also, high amount of common lead affects uncertainty to results because correct amount of common lead is challenging to estimate. Models are being used to determine the amount of common lead.

Köykkä et al. (2019) provided comprehensive summary of evolution of the Paleoproterozoic supracrustal units within the Fennoscandian shield. Among others, Kumpu group rocks and their detrital zircon characteristics, representing the youngest sedimentary strata in these supracrustal unit, were discussed. One peculiarities of the detrital zircon population found from the Kumpu group rocks, is the age population between 2.25-2.22 Ga. This age range can be only found from the Kumpu group rocks and it is believed to represent period of tectono-magmatic lull or shutdown, characterized by the decreasing activity of global-scale magmatism and orogenic activity (Köykkä et al., 2019 and references therein). Only after the onset of the thrust belt development during the Svecofennian orogeny, zircon ages of the 2.3-2.2 Ga appear to the sedimentary material within the supracrustal belts. In this study, the samples analyzed was found to contain zircon population representing this period of tectono-magmatic shutdown. Samples are containing age populations between 2.05-2.00 Ga. According to the Köykkä et al., (2019), coeval felsic porphyries and mafic intrusions of this age within the Central Lapland belt (Kitilä suite and Savukoski group) is probably the local source for the sedimentary material of this age. All other samples except 120059_A and 120071_A are altered quartzites and their major population occur between 1945-1905 Ma. Zircon populations of these ages found in this study are reported also in previous studies within the supracrustal units (Ranta et al., 2015; Köykkä et al., 2019). The felsic magmatism in the Lapland Granulite belt is potential source for the material of this age.

The youngest detrital zircon populations in this current study falls between 1.9-1.86 Ga. This age group is represented widely in the northern Fennoscandia by voluminous felsic plutonic rocks and similar ages are found in the Kumpu group rocks and matching units within the other supracrustal belts (see Köykkä et al., 2019).

Samples 120059_A and 120071_A represents conglomeratic rocks. These two samples have slightly older major population than other samples, around 2015 Ma and their maximum deposit ages are 1910 ± 10 Ma (120059_A) and 1919 ± 5 Ma (120071_A). Conglomerates seem to lack the age population <1.90 Ga which seems to indicate the deposition earlier compared to the quartzitic rocks.

According Lahtinen et al., (2015), the zircon ages 1.89-1.88 Ga are problematic difficulty proofing if zircons are detrital or metamorphic in origin. Lahtinen et al., (2015), interpreted in their study, zircon population between 1.86-1.85 Ga as metamorphic

because zircons have abundant metamorphic overgrowths. This metamorphic event has also been recorded in the Masugnabyrn area located in west of Pajala (Bergman et al., 2006). According to Lahtinen et al., (2015), there probably has been some metamorphic overgrowth of zircons also between 1.92-1.90 Ga. In this study, some zircon grains show clearly bimodal age distribution between core and rim, with core yielding older, Archean ages and rims younger ~1.93-1.90 Ga ages (Figure 11). In these cases, the zircons are clearly showing metamorphic overgrowth and cannot be interpreted to be from primary source.

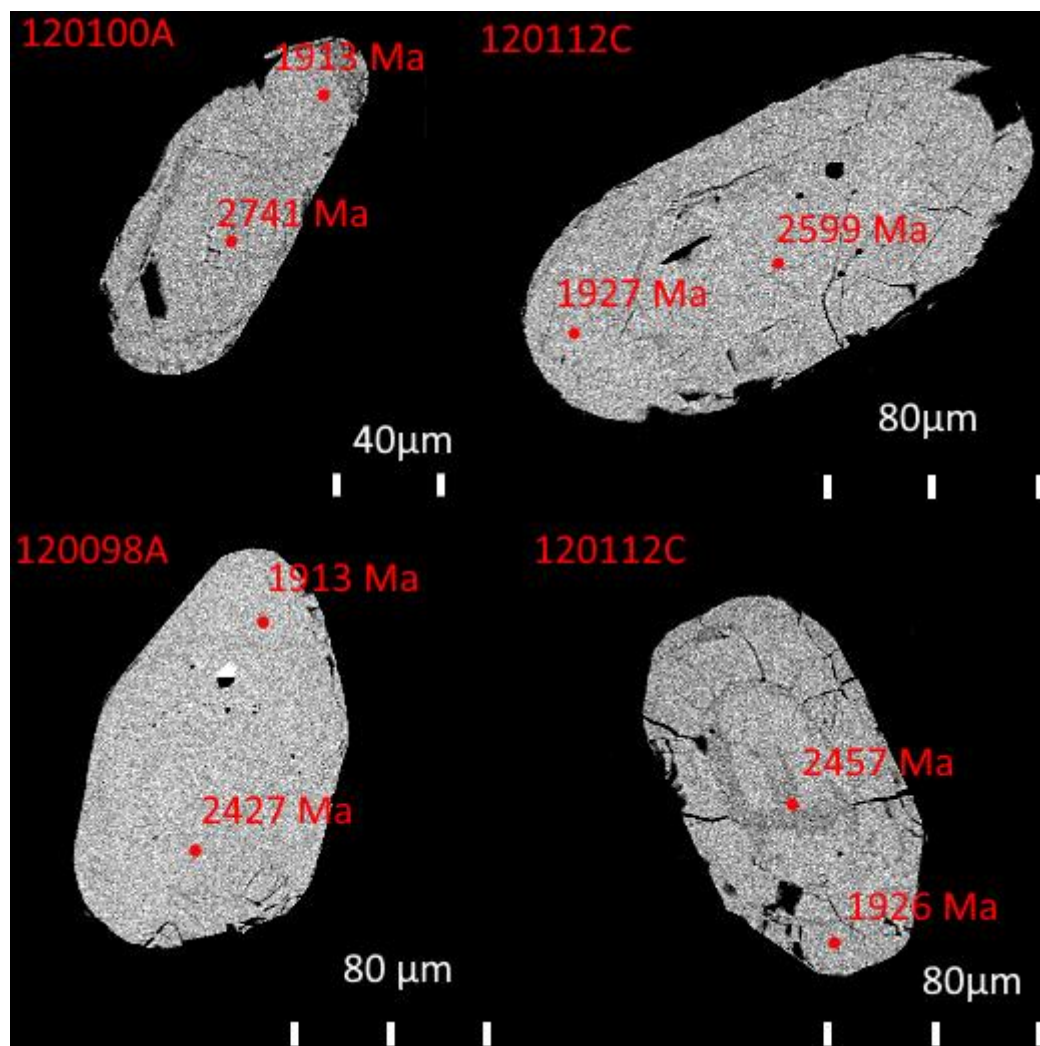


Figure 11. The two different ages points from each zircon grain which have circumferential structure. One age is from the centrum of the grain and another one is from the rim of the grain. Ages from the rims are probably metamorphic ages due to metamorphic overgrowths.

Overall, Comparing the overview of the geochronological studies represented by Köykkä et al., (2019), samples in this study are comparable to the Kumpu group metasedimentary rocks and therefore, overall results of this study shows that the studied metasedimentary units within the Ikkari deposits can be correlated with the Kumpu group, the youngest sedimentary unit in the Central Lapland belt.

The metasedimentary samples in this study are situated within the Ikkari gold deposit. Gold deposition is clearly epigenetic in origin as it is characterized by structurally controlled gold in highly sheared rocks with interlayered package of altered ultramafics and metasedimentary rocks which seem to be hydrothermally altered after peak metamorphism (J-P Ranta, personal communication 2022). According to Molnar (2021) most of the gold deposited at the late- to post-orogenic stages in all Svecofennian provinces between 1.82-1.75 Ga. This is a common age of the gold in other Paleoproterozoic supracrustal belts in Fennoscandia (e.g. Ranta et al., 2018). Older ages for gold ore-formation have been reported from the Central Lapland belt. For example, the Suurikuusikko deposit in Central Lapland belt shows age of 1916 ± 19 Ma for gold bearing arsenopyrite (Wyche et al., 2015). This would imply that some of the gold was deposited during/before the sedimentation of the Kumpu group rocks. Age of the Ikkari Au deposition is not yet fully understood. Preliminary geochronological data implies late-orogenic timing (Ranta, unpublished). However, the true age distribution and possible multistage mineralization processes of the Ikkari are yet to be unraveled.

8. CONCLUSIONS

The samples represent altered quartzites and conglomerates. The conglomerate samples seem to be slightly older than the other samples in this study. Based on U-Pb ages of the detrital zircon populations of this study, samples can be correlated in to the Kumpu group, the youngest sedimentary unit in the Central Lapland belt.

9. ACKNOWLEDGEMENTS

I would like to thank for the following people helping me during the thesis project:

- My supervisor Jukka-Pekka Ranta for guiding me through this study.
- Charlotte Seabrook and personnel of Rupert Resources for giving the subject to me and helping through this project.
- Matti Kurhila from GTK for doing sample preparations and giving good advices to handling the results.
- My fellow students for giving me unforgettable student years.
- Maria and my family for support and encouragement to finish the Master thesis.

10. REFERENCES

- Andersen, T., Elburg, M. and Magwaza, B., 2019, Sources of bias in detrital zircon geochronology: Discordance, concealed lead loss and common lead correction, *Earth-Science Reviews*, Volume 197
- Babu, M., Somashekar, R., Kumar, S., Shivanna, K., Krishnamurthy, V. and Eappen, K., 2008, Concentration of uranium levels in groundwater, *International Journal of Environmental Science & Technology*, Volume 5, p. 263–266
- Belousova, E., Griffin, W. and O'Reilly, S., 2006, Zircon crystal morphology, trace element signatures and Hf isotope composition as a tool for petrogenetic modeling: examples from Eastern Australian granitoids. *Journal of Petrology*, Volume 47, 329–353.
- Bergman, S., Billström, K., Persson, P., Skiöld, T. and Evins, P., 2006, U–Pb age evidence for repeated Palaeoproterozoic metamorphism and deformation near the Pajala shear zone in the northern Fennoscandian shield GFF, Volume 128, p. 7-20
- Chiaradia, M., 2020, Gold endowments of porphyry deposits controlled by precipitation efficiency, *Nature Communications*, Volume 11, Article number: 248
- Condie, K., Belousova, E., Griffin, W. and Sircombe, K., 2009, Granitoid events in space and time: Constraints from igneous and detrital zircon age spectra, *Gondwana Research*, Volume 15, Issues 3–4, Pages 228-242
- Crowley, Q., Heron, K., Riggs, N. and Kamber, B., 2014, Chemical abrasion applied to LA-ICP-MS U-Pb zircon geochronology, *Minerals*, Volume 4, p. 503-518
- Cuney, M., 2021, *Encyclopedia of Geology* (second edition), Volume 5
- Dickinson, W. and Gehrels G., 2009, Use of U–Pb ages of detrital zircons to infer maximum depositional ages of strata: A test against a Colorado Plateau Mesozoic database, *Earth and Planetary Sciences Letters*, Volume 288, p. 115-125
- Dube, B., Gosselin, P., Hannington, M., and Galley, A., 2007, Gold-rich volcanogenic massive sulphide deposits, *Geological Association of Canada, Mineral Deposits Division*, p. 75-94
- Eilu, P., Chapter 5.1 - Overview on Gold Deposits in Finland, *Mineral Deposits of Finland*, p. 377-410
- Gehrels, G., 2014, Detrital Zircon U-Pb Geochronology Applied to Tectonics, *Annual Review of Earth and Planetary Sciences*, Volume 42, p. 127-149
- Groves, D., Goldfarb, R., Gebre-Mariam, M., Hagemann, S. and Robert, F., 1998, Orogenic gold deposits: A proposed classification in the context of their crustal distribution and relationship to other gold deposit types, *Ore Geology Reviews*, Volume 13, Issues 1–5, p. 7-27
- Groves, D., Bierlein, F., Meinert, L. and Hitzman, M., 2010, Iron Oxide Copper-Gold (IOCG) Deposits through Earth History: Implications for Origin, Lithospheric Setting, and Distinction from Other Epigenetic Iron Oxide Deposits, *Economic Geology*, Volume 105, p.641–654.
- Hanski, E., Huhma, H. and Vaasjoki, M., 2001, Geochronology of northern Finland: a summary and discussion, *Geological Survey of Finland, Special Paper 33*, p. 255-279

- Hanski, E. and Huhma, H., 2005, Precambrian Geology of Finland, Volume 14, Chapter 4 Central Lapland greenstone belt, p. 139-193
- Harrison, T., 2009, The Hadean Crust: Evidence from >4 Ga Zircons, Annual Review of Earth and Planetary Sciences, Volume 37, p.479-505
- Herrington, R. and Stanley C., 2001, Gold deposits, The Natural History Museum, London, UK
- Huhma, H., Mänttari, I., Peltonen, P., Kontinen, A., Halkoaho, T., Hanski, E., Hokkanen, T., Hölttä, P., Juopperi, H., Komunaho, J., Layahe, Y., Luukkonen, E., Pietikäinen, K., Pulkkinen, A., Sorjonen-Ward, P., Vaasjoki, M. and Whitehouse, M., 2012, The age of the Archaean greenstone belts in Finland. Geological Survey of Finland, Special Paper 54, 74–175
- Huhma, H., Hanski, E., Kontinen, A., Vuollo, J., Mänttari, I. and Lahaye, Y., 2018. Sm-Nd and U-Pb isotope geochemistry of the Palaeoproterozoic mafic magmatism in eastern and northern Finland, Geol. Surv. Finl., Bull., Volume 405
- John, D., Vikre, P., du Bray, E., Blakely, R., Rockwell, D., Mauk, J., Anderson, E. and Graybeal, F., 2010, Descriptive models for epithermal gold-silver deposits, Scientific Investigations Report 2010–5070–Q, U.S. Geological Survey
- Kesler, S. and Chryssoulis, S., 2002, Gold in porphyry copper deposits: Its abundance and fate, Ore Geology Reviews Volume 21(1-2), p. 103-124
- Kohn, M. and Kelly, N., 2018, Petrology and Geochronology of Metamorphic Zircon. Microstructural Geochronology: Planetary Records Down to Atom Scale, p. 35-61
- Köykkä, J., and Luukas, J., 2019. Keski-Lapin temaattinen kallioperätutkimus ja kartoitus 2019, Geologian tutkimuskeskus, Alueellinen geotieto (ALG), Rovaniemi, GTK:n työraportti 99/2019.
- Köykkä, J., Lahtinen, R., Huhma, H., 2019, Provenance evolution of the Paleoproterozoic metasedimentary coversequences in northern Fennoscandia: Age distribution, geochemistry, and zircon morphology, Precambrian Research, Volume 331
- Köykkä J. and Luukas J., 2021, Keski-Lapin litostratigrafia ja paleoproterotsooisen Sodankylän ryhmän kivilajiyksiköiden määrittely, GTK:n tutkimustyöraportti 13/2021
- Lahtinen, R., Huhma, H., Lahaye, Y., Jonsson, E., Manninen, T. Lauri, L., Bergman, S., Hellstöm, F., Niianen, T. and Nironen, M., 2015, New geochronological and Sm-Nd constraints across the Pajala shear zone of northern Fennoscandia: Reactivation of a Paleoproterozoic suture. Precambrian Research, Volume 256, p.102–119
- Lankvelt, A., Schneider, D., Biczok, J., McFarlane, C. and Hattori, K., 2016, Decoding Zircon Geochronology of Igneous and Alteration Events Based on Chemical and Microstructural Features: a Study from the Western Superior Province, Canada, Journal of Petrology, Volume 57, Issue 7, p. 1309–1334
- Lehtonen, M., Airo, M-L., Eilu, P., Hanski, E., Kortelainen, V., Lanne, E., Manninen, T., Rastas, P., Räsänen J. and Virransalo, P., 1998, Kittilän vihreäkivialueen geologia. Lapin vulkaniittiprojektin raportti. Summary: The stratigraphy, petrology and geochemistry of the Kittilä Sequences. Geological Survey of Finland, Special Paper 33, p. 229-246.

- Liu, Y., Hou Z., Zhang R., Wang P., Gao J. and Raschke M., 2019, Zircon Alteration as a Proxy for Rare Earth Element Mineralization Processes in Carbonatite-Nordmarkite Complexes of the Mianning-Dechang Rare Earth Element Belt, China, *Economic Geology*, Volume 114, p. 719–744.
- Luukas, J., Kousa, J., Nironen, M. and Vuollo, J. 2017. Major stratigraphic units in the bedrock of Finland, and an approach to tectonostratigraphic division. Geological Survey of Finland, Special Paper 60, 9-40, 9 figures, 1 table and 1 appendix
- Ludwig, K., 2003, User's manual for Isoplot/Ex, Version 3.00. A geochronological toolkit for Microsoft Excel. Berkeley Geochronology Center Special Publication No.4.
- MacDonald, J., 2013, Zircon—Earth's timekeeper, *Geology Today*, Volume 29, Issue 3, p.113-117
- Molnar, F., 2021 Orogenic gold mineral systems in Finland, *Mineral systems of Finland*, GTK
- Morton, A. and Hallsworth, C., 1999, Processes controlling the composition of heavy mineral assemblages in sandstones, *Sedimentary Geology*, Volume 124, Issues 1–4, Pages 3-29
- Müller, W., Shelley M., Miller, P. and Broude, S., 2009, Initial performance metrics of a new custom-designed ArF excimer LA-ICPMS system coupled to a two-volume laser-ablation cell. *Journal of Analytical Atomic Spectrometry*, Volume 24, p. 209-214
- Nasdala, L., Pidgeon, R., Wolf, D., 1996, Heterogeneous metamictization of zircon on a microscale, *Geochimica et Cosmochimica Acta*, Volume 60, p. 1091-1097
- Niiranen, T., 2015, A 3D structural model of the central and eastern part of the Kittilä terrane. Geological Survey of Finland, Research Report, Volume 90
- Nikula R., 1988, Palaeosedimentology of precambrian tidal virttiövaara and fluvial värttiövaara quartzite formations in Sodankylä, northern Finland, Geological Survey of Finland, Special Paper 5, p.177-188
- Patison, N., Salamis, G., and Kortelainen, V., 2007, The Suurikuusikko gold deposit: Project development summary of northern Europe's largest gold resource, *Gold in the Central Lapland Greenstone Belt, Finland*, Geological Survey of Finland, Special Paper 44, p. 125– 134
- Pirkle, F. and Podmeyer, D., 1993, Zircon: origin and uses, *transactions, Society for mining, metallurgy, and exploration, inc*, Volume 292
- Pupin, J., 1980, Zircon and granite petrology, *Contributions to Mineralogy and Petrology* Volume 73, p. 207–220
- Ranta, J., 2012, Peräpohjan liuskealueen pohjoisosan yksiköiden zirkoniajotus U-Pb-menetelmällä, University of Oulu, Faculty of Geosciences
- Ranta, J., Lauri, L., Hanski, E., Huhma, H., Lahaye, Y., Vanhanen, E., 2015, U–Pb and Sm–Nd isotopic constraints on the evolution of the Paleoproterozoic Peräpohja Belt, northern Finland, *Precambrian Research*, Volume 266, p. 246-259
- Ranta, J., Molnár, F., Hanski E. and Cook, N., 2018 Epigenetic gold occurrence in a Paleoproterozoic meta-evaporitic sequence in the Rompas-Rajapalot Au system, Peräpohja belt, northern Finland, *Bulletin of the Geological Society of Finland*, 90(1)

- Rasmussen B., 2005, Radiometric dating of sedimentary rocks: the application of diagenetic xenotime geochronology, *Earth-Science Reviews*, Volume 68, Issues 3–4, p. 197-243
- Rastas, P, Huhma, H., Hanski, E., Lehtonen, M.I., Härkönen, I., Kortelainen, V., Mänttari, I. and Paakkola, J., 2001, U-Pb isotopic studies on the Kittilä greenstone area, central Lapland, Finland. Geological Survey of Finland, Special Paper 33
- Richards, J. and Mumin, A., 2013, Magmatic-hydrothermal processes within an evolving Earth: Iron oxide-copper-gold and porphyry Cu ± Mo ± Au deposits, *Geology*, Volume 41, p. 767–770.
- Rubatto, D., Gebauer, D. and Compagnoni, R., 1999, Dating of eclogite-facies zircons: the age of Alpine metamorphism in the Sesia–Lanzo Zone (Western Alps), *Earth and Planetary Science Letters*, Volume 167, Issues 3–4, p. 141-158
- Rupert resources, 2021, Rupert Resources Reports Maiden Inferred Resource for Ikkari of 49 Million Tonnes Grading 2.5 Grams Per Tonne (3.95 Million Ounces of Gold), News, Rupert resources official web page
- Rupert resources, 2022, Ikkari discovery, Rupert Lapland project, Assets, Rupert resources official web page
- Saunders, J., Hofstra, A., Goldfarb, R. and Reed, M, 2014, Geochemistry of Hydrothermal Gold Deposits, *Treatise on Geochemistry (Second Edition) Volume 13*, p. 383-424
- Schoene, B., 2014, U–Th–Pb Geochronology, Princeton University, Elsevier
- Schneider, D., Bachtel, J. and Schmitt, A., 2012, Zircon Alteration in Wall Rock of Pamour and Hoyle Pond Au Deposits, Abitibi Greenstone Belt: Constraints on Timescales of Fluid Flow from Depth-Profiling Techniques. 2 Society of Economic Geologists, Inc. *Economic Geology*, Volume 107, p. 1043–1072
- Sharman, G., Sharman, J. and Sylvester, Z., 2018, detritalPy: A Python-based toolset for visualizing and analysing detrital geo-thermochronologic data, *The Depositional Record*, Volume 4, Issue 2 p. 202-215
- Spandler C., Hermann J. and Rubatto D., 2004, Exsolution of thortveitite, yttrialite, and xenotime during low-temperature recrystallization of zircon from New Caledonia, and their significance for trace element incorporation in zircon, *American Mineralogist*, Volume 89 p. 1795–1806.
- Stacey, J., and Kramers, J., 1975, Approximation of terrestrial lead isotope evolution by a two-stage model. *Earth and Planetary Science Letters* 26, p. 207-221.
- Tapia-Fernandez, H., Armstrong-altrin, J. and Selvaraj, K., 2017, Geochemistry and U–Pb geochronology of detrital zircons in the Brujas beach sands, Campeche, Southwestern Gulf of Mexico, Mexico, *Journal of South American Earth Sciences*, Volume 76, Pages 346-361
- Van Achterbergh, E., Ryan C., Jackson, S. and Griffin, W., 2001, Data reduction software for LA-ICP-MS, in: *Laser-Ablation ICPMS in the Earth Sciences – Principles and applications*, Mineralogical Association of Canada short course series, 29, St John, Newfoundland, Sylvester P. Ed., p. 239-243.

Vermeesch, P., 2021. *Isotope Geology Part I: Radiometric Geochronology*, London Geochronology Centre, University College London

Williams, I., 2001, Response of detrital zircon and monazite, and their U-Pb isotopic systems, to regional metamorphism and host-rock partial melting, Cooma Complex, southeastern Australia, *Aust. J. Earth Sci.*, Volume 48, p. 557–580.

Windley, B., 2007, *Developments in Precambrian Geology*, Volume 15, p. 3-7

Weihed, P., Eilu, P., Larsen, R., Stendal, H. and Tontti, M., 2008, Metallic mineral deposits in the Nordic countries, *Episodes*, 31, p.125-132

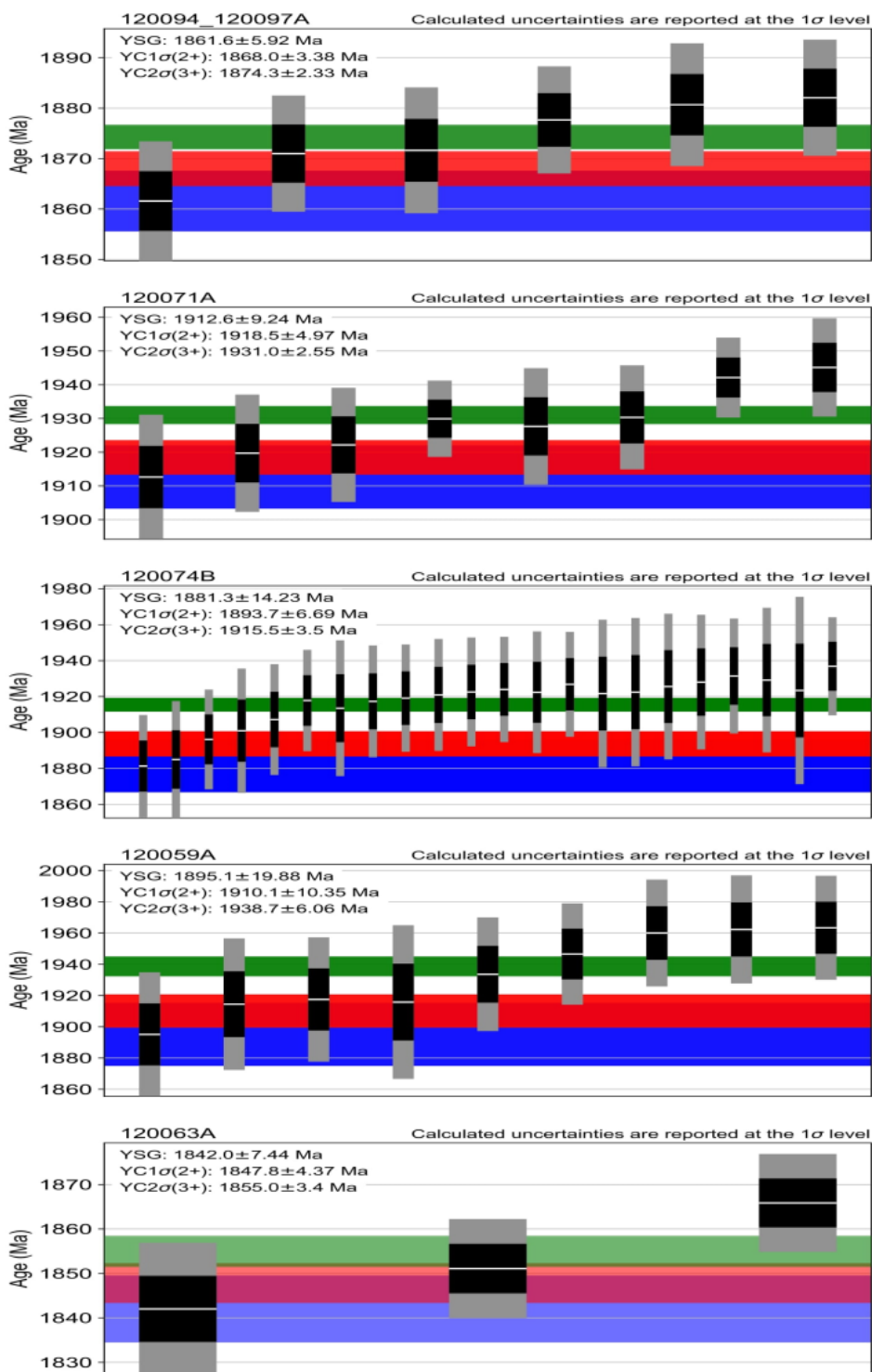
Wetherill, G., 1956, Discordant uranium-lead ages, I, *Eos, Transactions American Geophysical Union*, Volume 37, Issue 3 p. 320-326

Wu, Y. and Zheng, Y., 2004, Genesis of zircon and its constraints on interpretation of U-Pb age, *Chinese Science Bulletin* Volume 49 No. 15 p. 1554-1569

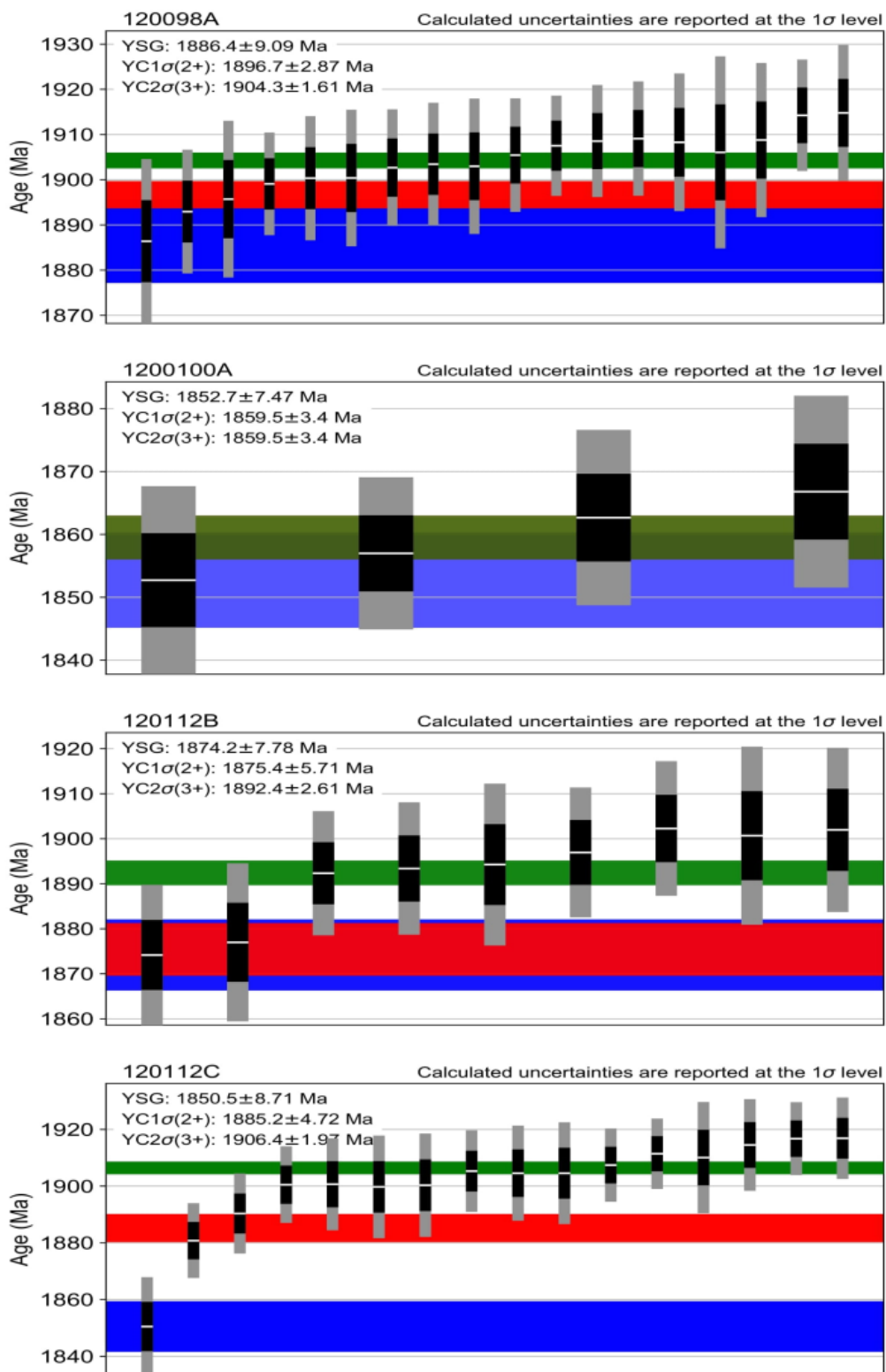
Wyche, N., Eilu, P., Koppström, K., Kortelainen, V., T. Niiranen, T. and Välimaa, J., 2015, Chapter 5.2 - The Suurikuusikko Gold Deposit (Kittilä Mine), Northern Finland, *Mineral Deposits of Finland*, p. 411-433

APPENDICES

Appendix 1(1). Result of maximum deposition age calculations.



Appendix 1(2). Result of maximum deposition age calculations.



Appendix 2(1) Morphology of the zircon grains

Sample ID	Description	Euhedral or not	Size	Sample ID	Description	Euhedral or not	Size
120059A_01	Angular	Euhedral	Medium	120059A_54	Rounded		Medium
120059A_02	Subrounded		Medium	120059A_55	Subrounded	Euhedral	Medium
120059A_03	Rounded		Medium	120059A_56	Rounded		Small
120059A_04	Subrounded		Large	120059A_57	Angular		Small
120059A_05	Subrounded		Medium	120059A_58	Angular		Medium
120059A_06	Subrounded		Small	120059A_59	Subrounded		Medium
120059A_07	Rounded		Medium	120059A_60	Subrounded		Medium
120059A_08	Subrounded		Medium	120059A_61	Subrounded		Medium
120059A_09	Rounded		Small	120059A_62	Angular	Euhedral	Medium
120059A_10	Subrounded		Medium	120059A_63	Subrounded		Medium
120059A_11	Angular		Small	120059A_64	Rounded		Small
120059A_12	Angular		Medium	120059A_65	Subrounded		Medium
120059A_13	Rounded		Medium	120059A_66	Subrounded		Medium
120059A_14	Rounded		Medium	120059A_67	Angular		Medium
120059A_15	Subrounded		Medium	120059A_68	Rounded		Medium
120059A_16	Rounded		Large	120059A_69	Subrounded		Medium
120059A_17	Subrounded		Small	120059A_70	Subrounded		Medium
120059A_18	Subrounded		Medium	120059A_71	Subrounded		Small
120059A_19	Subrounded	Euhedral	Small	120059A_72	Rounded		Small
120059A_20	Rounded		Medium	120059A_73	Rounded		Small
120059A_21	Subrounded		Small	120059A_74	Subrounded	Euhedral	Medium
120059A_22	Subrounded		Medium	120059A_75	Subrounded		Small
120059A_23	Subrounded		Small	120059A_76	Subrounded	Euhedral	Medium
120059A_24	Angular		Medium	120059A_77	Rounded	Euhedral	Medium
120059A_25	Subrounded		Medium	120059A_78			
120059A_26	Subrounded		Small	120059A_79	Subrounded	Euhedral	Medium
120059A_27	Angular		Medium	120059A_80	Angular		Small
120059A_28	Rounded		Small	120059A_81	Subrounded		Medium
120059A_29	Rounded		Medium	120059A_82	Subrounded	Euhedral	Medium
120059A_30	Subrounded		Medium	120059A_83	Rounded		Small
120059A_31	Angular		Medium	120059A_84	Subrounded		Small
120059A_32	Angular		Medium	120059A_85	Angular	Euhedral	Medium
120059A_33	Angular		Medium	120059A_86	Rounded		Medium
120059A_34	Rounded		Medium	120059A_87	Rounded		Medium
120059A_35	Rounded		Small	120059A_88	Subrounded		Medium
120059A_36	Rounded		Small	120059A_89	Subrounded	Euhedral	Medium
120059A_37	Angular	Euhedral	Small	120059A_90	Subrounded		Small
120059A_38	Rounded		Large	120059A_91	Subrounded		Large
120059A_39	Subrounded		Medium	120059A_92	Angular		Large
120059A_40	Subrounded	Euhedral	Medium	120059A_93	Subrounded		Medium
120059A_41	Subrounded		Medium	120059A_94	Angular		Small
120059A_42	Angular		Small	120059A_95	Subrounded		Small
120059A_43	Rounded		Medium	120059A_96	Angular		Small
120059A_44	Angular		Small	120059A_97	Subrounded		Small
120059A_45	Subrounded		Medium	120059A_98	Subrounded		Medium
120059A_46	Angular		Small	120059A_99	Angular		Medium
120059A_47	Subrounded	Euhedral	Large	120059A_100	Subrounded		Small
120059A_48	Subrounded		Medium	120059A_101	Subrounded		Medium
120059A_49	Subrounded	Euhedral	Medium	120059A_102	Subrounded		Medium
120059A_50	Rounded		Medium	120059A_103	Angular	Euhedral	Medium
120059A_51	Subrounded	Euhedral	Small	120059A_104	Subrounded		Medium
120059A_52	Rounded		Medium	120059A_105	Subrounded		Medium
120059A_53	Rounded		Medium				

Appendix 2(2) Morphology of the zircon grains.

Sample ID	Description	Euhedral or not	Size	Sample ID	Description	Euhedral or not	Size
120063A_01	Subrounded	Euhedral	Small	120063A_53	Rounded		Large
120063A_02	Angular	Euhedral	Medium	120063A_54	Subrounded		Medium
120063A_03	Subrounded	Euhedral	Medium	120063A_55	Subrounded		Small
120063A_04	Rounded		Medium	120063A_56	Subrounded	Euhedral	Medium
120063A_05	Rounded		Medium	120063A_57	Subrounded	Euhedral	Large
120063A_06	Angular	Euhedral	Medium	120063A_58	Rounded		Medium
120063A_07	Subrounded		Medium	120063A_59	Subrounded	Euhedral	Medium
120063A_08	Rounded		Small	120063A_60	Rounded		Medium
120063A_09	Angular	Euhedral	Medium	120063A_61	Rounded		Small
120063A_10	Rounded		Medium	120063A_62	Subrounded		Medium
120063A_11	Rounded		Medium	120063A_63	Subrounded		Medium
120063A_12	Rounded		Medium	120063A_64	Subrounded	Euhedral	Medium
120063A_13	Rounded	Euhedral	Small	120063A_65	Rounded	Euhedral	Small
120063A_14	Subrounded		Medium	120063A_66	Subrounded		Medium
120063A_15	Rounded		Medium	120063A_67	Rounded		Medium
120063A_16	Rounded		Medium	120063A_68	Rounded		Large
120063A_17	Rounded		Large	120063A_69	Rounded		Medium
120063A_18	Rounded		Medium	120063A_70	Angular		Medium
120063A_19	Subrounded	Euhedral	Medium	120063A_71	Rounded		Medium
120063A_20	Angular		Small	120063A_72	Angular		Medium
120063A_21	Subrounded	Euhedral	Medium	120063A_73	Subrounded		Medium
120063A_22	Rounded		Small	120063A_74	Rounded		Medium
120063A_23	Rounded		Medium	120063A_75	Rounded		Medium
120063A_24	Subrounded	Euhedral	Medium	120063A_76	Angular		Small
120063A_25	Angular	Euhedral	Medium	120063A_77	Subrounded	Euhedral	Small
120063A_26	Subrounded		Small	120063A_78	Rounded		Small
120063A_27	Rounded		Medium	120063A_79	Subrounded		Small
120063A_28	Rounded	Euhedral	Medium	120063A_80	Rounded		Medium
120063A_29	Subrounded	Euhedral	Medium	120063A_81	Subrounded		Small
120063A_30	Angular		Small	120063A_82	Subrounded	Euhedral	Medium
120063A_31	Subrounded	Euhedral	Medium	120063A_83	Subrounded	Euhedral	Medium
120063A_32	Rounded		Medium	120063A_84	Rounded		Medium
120063A_33	Angular		Medium	120063A_85	Rounded		Large
120063A_34	Rounded		Medium	120063A_86	Subrounded	Euhedral	Medium
120063A_35	Subrounded	Euhedral	Small	120063A_87	Subrounded		Small
120063A_36	Angular		Small	120063A_88	Subrounded		Medium
120063A_37	Angular		Medium	120063A_89	Subrounded		Medium
120063A_38	Subrounded		Medium	120063A_90	Angular	Euhedral	Large
120063A_39	Subrounded	Euhedral	Medium	120063A_91	Subrounded		Medium
120063A_40	Subrounded		Small	120063A_92	Subrounded		Medium
120063A_41	Subrounded	Euhedral	Medium	120063A_93	Rounded		Large
120063A_42	Subrounded		Small	120063A_94	Angular		Medium
120063A_43	Rounded		Small	120063A_95	Subrounded		Medium
120063A_44	Rounded		Medium	120063A_96	Rounded		Medium
120063A_45	Angular		Medium	120063A_97	Rounded		Large
120063A_46	Subrounded	Euhedral	Medium	120063A_98	Rounded		Small
120063A_47	Rounded		Large	120063A_99	Subrounded		Medium
120063A_48	Subrounded		Medium	120063A_100	Rounded		Small
120063A_49	Rounded	Euhedral	Medium	120063A_101	Subrounded		Small
120063A_50	Rounded	Euhedral	Medium	120063A_102	Subrounded		Small
120063A_51	Rounded		Medium				
120063A_52	Rounded	Euhedral	Medium				

Appendix 2(3) Morphology of the zircon grains.

Sample number	Description	Euhedral or not	Size	Sample number	Description	Euhedral or not	Size
120071A_01	Angular		Medium	120071A_52	Subrounded	Euhedral	Medium
120071A_02	Subrounded	Euhedral	Medium	120071A_53	Subrounded		Small
120071A_03	Angular	Euhedral	Medium	120071A_54	Angular		Medium
120071A_04	Rounded		Medium	120071A_55	Angular	Euhedral	Medium
120071A_05	Angular	Euhedral	Small	120071A_56	Subrounded		Small
120071A_06	Subrounded	Euhedral	Small	120071A_57	Subrounded	Euhedral	Small
120071A_07	Rounded		Small	120071A_58	Rounded		Medium
120071A_08	Rounded		Medium	120071A_59	Subrounded	Euhedral	Small
120071A_09	Angular		Small	120071A_60	Angular	Euhedral	Small
120071A_10	Angular		Medium	120071A_61	Angular	Euhedral	Medium
120071A_11	Subrounded		Small	120071A_62	Rounded		Medium
120071A_12	Subrounded	Euhedral	Small	120071A_63	Angular		Medium
120071A_13	Subrounded	Euhedral	Medium	120071A_64	Angular	Euhedral	Large
120071A_14a	Subrounded	Euhedral	Medium	120071A_65	Angular		Small
120071A_14b	Rim	Euhedral	Medium	120071A_66	Angular		Medium
120071A_15	Subrounded		Medium	120071A_67	Angular		Small
120071A_16	Angular		Small	120071A_68a	Subrounded	Euhedral	Medium
120071A_17	Angular		Medium	120071A_68b	Rim		Medium
120071A_18	Subrounded	Euhedral	Medium	120071A_69	Angular		Medium
120071A_19	Subrounded	Euhedral	Medium	120071A_70	Angular	Euhedral	Small
120071A_20	Angular		Medium	120071A_71	Subrounded		Medium
120071A_21	Angular	Euhedral	Small	120071A_72	Subrounded		Medium
120071A_22	Subrounded	Euhedral	Small	120071A_73	Subrounded		Medium
120071A_23	Subrounded	Euhedral	Small	120071A_74	Subrounded		Medium
120071A_24	Subrounded		Small	120071A_75	Rounded		Medium
120071A_25	Angular	Euhedral	Medium	120071A_76	Rounded		Small
120071A_26	Subrounded		Small	120071A_77	Subrounded		Small
120071A_27	Subrounded		Medium	120071A_78	Subrounded		Medium
120071A_28	Subrounded	Euhedral	Medium	120071A_79	Angular		Medium
120071A_29	Subrounded	Euhedral	Small	120071A_80	Subrounded		Medium
120071A_30	Subrounded	Euhedral	Small	120071A_81	Subrounded		Medium
120071A_31	Subrounded		Medium	120071A_82	Rounded		Medium
120071A_32	Subrounded		Medium	120071A_83	Subrounded		Small
120071A_33	Subrounded	Euhedral	Small	120071A_84	Subrounded	Euhedral	Medium
120071A_34	Angular		Small	120071A_85	Subrounded		Large
120071A_35	Angular		Medium	120071A_86	Subrounded	Euhedral	Medium
120071A_36	Rounded		Small	120071A_87	Subrounded		Medium
120071A_37	Subrounded	Euhedral	Medium	120071A_88	Subrounded	Euhedral	Medium
120071A_38	Subrounded		Large	120071A_89	Rounded		Medium
120071A_39a	Angular	Euhedral	Large	120071A_90	Angular		Medium
120071A_39b	Rim		Large	120071A_91	Angular	Euhedral	Small
120071A_40	Angular		Medium	120071A_92	Subrounded		Medium
120071A_41	Subrounded		Small	120071A_93	Angular	Euhedral	Medium
120071A_42	Subrounded		Small	120071A_94	Angular	Euhedral	Medium
120071A_43	Angular		Medium	120071A_95	Subrounded		Small
120071A_44	Rounded		Medium	120071A_96	Subrounded	Euhedral	Medium
120071A_45	Rounded		Medium	120071A_97	Subrounded		Small
120071A_46	Subrounded		Medium	120071A_98	Rounded		Medium
120071A_47	Subrounded		Medium	120071A_99	Rounded		Medium
120071A_48	Subrounded		Small	120071A_100	Angular	Euhedral	Medium
120071A_49	Subrounded		Medium	120071A_101	Rounded		Medium
120071A_50	Angular	Euhedral	Medium				
120071A_51	Subrounded		Medium				

Appendix 2(4) Morphology of the zircon grains.

Sample ID	Description	Euhedral or not	Size	Sample ID	Description	Euhedral or not	Size
120074B-a_01a	Subrounded	Euhedral	Medium	120074B-a_54	Rounded		Medium
120074B-a_01b	Rim		Medium	120074B-a_55	Rounded		Small
120074B-a_02	Subrounded	Euhedral	Large	120074B-a_56	Rounded		Medium
120074B-a_03	Rounded		Medium	120074B-a_57	Rounded		Small
120074B-a_04	Subrounded		Medium	120074B-a_58	Rounded	Euhedral	Medium
120074B-a_05	Rounded		Small	120074B-a_59	Angular		Small
120074B-a_06	Subrounded		Large	120074B-a_60	Rounded		Medium
120074B-a_07	Subrounded	Euhedral	Small	120074B-a_61	Rounded		Medium
120074B-a_08	Rounded		Medium	120074B-a_62	Rounded		Small
120074B-a_09	Subrounded		Medium	120074B-a_63	Subrounded		Medium
120074B-a_10	Angular		Small	120074B-a_64	Rounded		Medium
120074B-a_11	Subrounded		Small	120074B-a_65	Rounded		Medium
120074B-a_12	Subrounded		Medium	120074B-a_66	Subrounded	Euhedral	Medium
120074B-a_13	Subrounded		Medium	120074B-a_67	Subrounded	Euhedral	Medium
120074B-a_14	Subrounded		Medium	120074B-a_68	Rounded		Medium
120074B-a_15	Rounded		Medium	120074B-a_69	Rounded		Medium
120074B-a_16	Subrounded		Medium	120074B-a_70	Subrounded		Medium
120074B-a_17	Subrounded		Medium	120074B-a_71	Subrounded		Medium
120074B-a_18	Subrounded	Euhedral	Large	120074B-a_72	Rounded		Medium
120074B-a_19	Subrounded		Medium	120074B-a_73	Subrounded	Euhedral	Medium
120074B-a_20	Rounded		Small	120074B-a_74	Rounded		Large
120074B-a_21	Angular		Medium	120074B-a_75	Rounded		Small
120074B-a_22	Subrounded		Small	120074B-a_76	Rounded		Small
120074B-a_23	Subrounded	Euhedral	Large	120074B-a_77	Subrounded		Medium
120074B-a_24	Rounded		Small	120074B-a_78	Rounded		Medium
120074B-a_25	Angular	Euhedral	Small	120074B-a_79	Subrounded		Medium
120074B-a_26	Rounded	Euhedral	Medium	120074B-a_80	Subrounded		Small
120074B-a_27	Subrounded	Euhedral	Medium	120074B-a_81	Subrounded		Medium
120074B-a_28	Rounded		Medium	120074B-a_82	Subrounded	Euhedral	Medium
120074B-a_29	Subrounded	Euhedral	Medium	120074B-a_83	Rounded	Euhedral	Large
120074B-a_30	Rounded	Euhedral	Large	120074B-a_84	Subrounded		Medium
120074B-a_31	Subrounded		Small	120074B-a_85	Rounded		Medium
120074B-a_32	Rounded	Euhedral	Medium	120074B-a_86	Subrounded		Medium
120074B-a_33	Subrounded	Euhedral	Medium	120074B-a_87	Rounded		Medium
120074B-a_34	Rounded		Medium	120074B-a_88	Rounded		Medium
120074B-a_35	Angular		Medium	120074B-a_89	Rounded		Medium
120074B-a_36	Rounded		Medium	120074B-a_90	Subrounded		Small
120074B-a_37	Subrounded	Euhedral	Medium	120074B-a_91	Rounded		Small
120074B-a_38	Rounded		Medium	120074B-a_92	Rounded		Small
120074B-a_39	Rounded		Medium	120074B-a_93	Rounded	Euhedral	Medium
120074B-a_40	Subrounded	Euhedral	Small	120074B-a_94	Rounded	Euhedral	Medium
120074B-a_41	Subrounded	Euhedral	Medium	120074B-a_95	Subrounded		Medium
120074B-a_42	Rounded		Medium	120074B-a_96	Rounded		Medium
120074B-a_43	Rounded		Small	120074B-a_97	Rounded	Euhedral	Medium
120074B-a_44	Rounded		Medium	120074B-a_98	Subrounded		Medium
120074B-a_45	Subrounded	Euhedral	Large	120074B-a_99	Subrounded		Medium
120074B-a_46	Rounded		Medium	120074B-a_100	Subrounded		Medium
120074B-a_47	Rounded		Small	120074B-a_101	Rounded		Medium
120074B-a_48	Rounded		Small	120074B-a_102	Subrounded		Medium
120074B-a_49	Rounded		Medium	120074B-a_103	Subrounded		Medium
120074B-a_50	Subrounded		Medium	120074B-a_104	Rounded		Medium
120074B-a_51	Subrounded	Euhedral	Medium	120074B-a_105	Subrounded		Medium
120074B-a_52	Rounded	Euhedral	Medium	120074B-a_106	Subrounded	Euhedral	Large
120074B-a_53	Rounded		Medium				

Appendix 2(5) Morphology of the zircon grains.

Sample ID	Description	Euhedral or not	Size	Sample ID	Description	Euhedral or not	Size
120097-120094A_01	Subrounded	Euhedral	Medium	120097-120094A_54	Subrounded	Euhedral	Medium
120097-120094A_02	Rounded		Medium	120097-120094A_55	Subrounded	Euhedral	Medium
120097-120094A_03	Rounded		Medium	120097-120094A_56	Rounded		Small
120097-120094A_04	Subrounded		Medium	120097-120094A_57	Rounded	Euhedral	Medium
120097-120094A_05	Subrounded		Medium	120097-120094A_58	Rounded	Euhedral	Small
120097-120094A_06	Subrounded		Small	120097-120094A_59	Subrounded		Medium
120097-120094A_07	Subrounded		Medium	120097-120094A_60	Subrounded		Small
120097-120094A_08	Subrounded	Euhedral	Medium	120097-120094A_61	Subrounded		Medium
120097-120094A_09	Subrounded	Euhedral	Medium	120097-120094A_62	Rounded	Euhedral	Medium
120097-120094A_10	Rounded		Medium	120097-120094A_63	Subrounded	Euhedral	Medium
120097-120094A_11	Subrounded	Euhedral	Medium	120097-120094A_64	Subrounded		Small
120097-120094A_12	Rounded	Euhedral	Medium	120097-120094A_65	Rounded		Medium
120097-120094A_13a	Subrounded		Large	120097-120094A_66	Rounded		Medium
120097-120094A_13b	Rim		Large	120097-120094A_67	Rounded		Small
120097-120094A_14	Subrounded		Medium	120097-120094A_68	Rounded		Large
120097-120094A_15	Subrounded	Euhedral	Medium	120097-120094A_69	Subrounded		Medium
120097-120094A_16	Rounded		Small	120097-120094A_70	Subrounded		Medium
120097-120094A_17	Rounded		Medium	120097-120094A_71	Rounded		Small
120097-120094A_18	Rounded		Small	120097-120094A_72	Subrounded	Euhedral	Large
120097-120094A_19	Rounded		Medium	120097-120094A_73	Subrounded		Medium
120097-120094A_20	Angular	Euhedral	Medium	120097-120094A_74	Angular		Small
120097-120094A_21	Subrounded		Large	120097-120094A_75	Subrounded		Medium
120097-120094A_22	Rounded		Small	120097-120094A_76	Subrounded		Small
120097-120094A_23	Subrounded	Euhedral	Medium	120097-120094A_77	Subrounded		Medium
120097-120094A_24	Subrounded		Small	120097-120094A_78	Subrounded		Medium
120097-120094A_25	Rounded		Small	120097-120094A_79	Rounded		Medium
120097-120094A_26	Rounded	Euhedral	Large	120097-120094A_80	Subrounded		Medium
120097-120094A_27	Rounded		Small	120097-120094A_81	Subrounded		Small
120097-120094A_28	Subrounded	Euhedral	Medium	120097-120094A_82	Rounded	Euhedral	Medium
120097-120094A_29	Subrounded	Euhedral	Large	120097-120094A_83	Rounded		Medium
120097-120094A_30	Subrounded	Euhedral	Medium	120097-120094A_84	Subrounded	Euhedral	Medium
120097-120094A_31	Rounded		Medium	120097-120094A_85	Rounded		Medium
120097-120094A_32	Rounded		Large	120097-120094A_86	Rounded		Medium
120097-120094A_33	Subrounded		Medium	120097-120094A_87	Subrounded		Medium
120097-120094A_34	Subrounded		Large	120097-120094A_88	Rounded		Medium
120097-120094A_35	Rounded	Euhedral	Medium	120097-120094A_89	Subrounded		Medium
120097-120094A_36	Rounded		Medium	120097-120094A_90	Rounded		Medium
120097-120094A_37	Subrounded		Medium	120097-120094A_91	Subrounded		Medium
120097-120094A_38	Rounded		Small	120097-120094A_92	Subrounded	Euhedral	Small
120097-120094A_39	Subrounded		Medium	120097-120094A_93	Subrounded		Medium
120097-120094A_40	Subrounded		Medium	120097-120094A_94	Rounded		Medium
120097-120094A_41	Rounded	Euhedral	Large	120097-120094A_95	Rounded		Medium
120097-120094A_42	Rounded	Euhedral	Medium	120097-120094A_96	Subrounded		Small
120097-120094A_43	Rounded		Medium	120097-120094A_97	Rounded		Small
120097-120094A_44	Subrounded	Euhedral	Large	120097-120094A_98	Rounded		Medium
120097-120094A_45	Rounded	Euhedral	Medium	120097-120094A_99	Rounded		Small
120097-120094A_46	Subrounded		Medium	120097-120094A_100	Subrounded		Small
120097-120094A_47	Rounded		Small	120097-120094A_101	Subrounded		Small
120097-120094A_48	Subrounded		Small	120097-120094A_102	Angular		Medium
120097-120094A_49	Rounded		Medium	120097-120094A_103	Rounded		Medium
120097-120094A_50	Rounded		Medium	120097-120094A_104	Subrounded		Small
120097-120094A_51	Subrounded	Euhedral	Medium	120097-120094A_105	Subrounded	Euhedral	Medium
120097-120094A_52	Subrounded		Small	120097-120094A_106	Subrounded		Large
120097-120094A_53	Subrounded	Euhedral	Medium				

Appendix 2(6) Morphology of the zircon grains.

Sample ID	Description	Euhedral or not	Size	Sample ID	Description	Euhedral or not	Size
120098A_01	Subrounded		Medium	120098A_54	Subrounded		Large
120098A_02	Angular		Small	120098A_55	Rounded		Medium
120098A_03	Rounded		Large	120098A_56	Rounded		Small
120098A_04	Subrounded		Medium	120098A_57	Rounded		Medium
120098A_05	Rounded		Small	120098A_58	Rounded	Euhedral	Medium
120098A_06	Subrounded		Small	120098A_59	Subrounded		Small
120098A_07	Subrounded	Euhedral	Medium	120098A_60	Rounded		Small
120098A_08	Rounded		Small	120098A_61	Rounded		Small
120098A_09	Rounded		Small	120098A_62	Subrounded	Euhedral	Medium
120098A_10	Rounded		Large	120098A_63	Rounded		Medium
120098A_11	Subrounded	Euhedral	Small	120098A_64	Subrounded	Euhedral	Small
120098A_12	Subrounded		Small	120098A_65	Subrounded		Medium
120098A_13	Subrounded		Small	120098A_66	Subrounded		Medium
120098A_14	Subrounded		Medium	120098A_67	Subrounded		Medium
120098A_15	Rounded		Large	120098A_68	Rounded		Medium
120098A_16	Rounded		Medium	120098A_69	Rounded		Medium
120098A_17	Subrounded	Euhedral	Medium	120098A_70	Angular		Medium
120098A_18	Angular		Small	120098A_71	Rounded		Medium
120098A_19	Rounded		Small	120098A_72	Subrounded	Euhedral	Medium
120098A_20	Rounded		Small	120098A_73	Subrounded		Medium
120098A_21	Angular	Euhedral	Medium	120098A_74	Subrounded		Medium
120098A_22	Angular		Medium	120098A_75	Subrounded	Euhedral	Medium
120098A_23	Rounded		Small	120098A_76	Subrounded		Medium
120098A_24	Subrounded		Medium	120098A_77	Rounded	Euhedral	Medium
120098A_25	Subrounded		Medium	120098A_78	Rounded		Small
120098A_26	Subrounded		Medium	120098A_79	Subrounded		Small
120098A_27	Subrounded		Medium	120098A_80	Subrounded	Euhedral	Large
120098A_28	Subrounded		Medium	120098A_81	Subrounded		Medium
120098A_29a	Subrounded		Medium	120098A_82	Rounded		Medium
120098A_29b	Rim		Medium	120098A_83	Rounded		Medium
120098A_30	Rounded		Medium	120098A_84	Rounded		Medium
120098A_31	Subrounded		Medium	120098A_85	Rounded		Small
120098A_32	Subrounded		Medium	120098A_86	Subrounded	Euhedral	Large
120098A_33	Subrounded		Medium	120098A_87	Rounded		Small
120098A_34	Subrounded		Small	120098A_88	Rounded		Small
120098A_35	Subrounded		Small	120098A_89	Rounded		Small
120098A_36	Rounded	Euhedral	Large	120098A_90	Subrounded		Small
120098A_37	Subrounded		Medium	120098A_91	Rounded		Medium
120098A_38	Subrounded		Small	120098A_92	Rounded	Euhedral	Large
120098A_39	Rounded		Medium	120098A_93	Subrounded	Euhedral	Medium
120098A_40	Subrounded		Small	120098A_94	Subrounded		Medium
120098A_41	Subrounded		Large	120098A_95	Rounded		Medium
120098A_42a	Rounded		Medium	120098A_96	Subrounded		Medium
120098A_42b	Rim		Medium	120098A_97	Rounded	Euhedral	Medium
120098A_43	Angular		Small	120098A_98	Subrounded		Small
120098A_44	Rounded		Small	120098A_99	Subrounded		Small
120098A_45	Subrounded		Small	120098A_100	Subrounded		Small
120098A_46	Subrounded		Small	120098A_101	Subrounded	Euhedral	Medium
120098A_47	Rounded		Small	120098A_102	Subrounded		Medium
120098A_48	Subrounded		Medium	120098A_103	Rounded		Medium
120098A_49	Subrounded		Medium	120098A_104	Rounded		Medium
120098A_50	Angular	Euhedral	Medium	120098A_105	Subrounded	Euhedral	Medium
120098A_51	Subrounded		Small	120098A_106	Rounded		Medium
120098A_52	Subrounded		Medium	120098A_107	Subrounded		Small
120098A_53	Subrounded		Large				

Appendix 2(7) Morphology of the zircon grains.

Sample ID	Description	Euhedral or not	Size	Sample ID	Description	Euhedral or not	Size
120100A_01	Subrounded		Medium	120100A_56	Subrounded		Medium
120100A_02	Rounded		Medium	120100A_57	Subrounded		Medium
120100A_03	Rounded		Medium	120100A_58	Subrounded		Medium
120100A_04	Subrounded		Small	120100A_59	Subrounded		Medium
120100A_05	Subrounded		Large	120100A_60	Subrounded	Euhedral	Medium
120100A_06	Subrounded	Euhedral	Medium	120100A_61	Subrounded	Euhedral	Medium
120100A_07	Rounded		Small	120100A_62	Rounded		Medium
120100A_08	Subrounded		Large	120100A_63	Subrounded		Small
120100A_09	Angular		Small	120100A_64	Subrounded	Euhedral	Medium
120100A_10a	Rounded		Large	120100A_65	Subrounded	Euhedral	Medium
120100A_10b	Rim		Large	120100A_66	Rounded		Small
120100A_11	Subrounded		Small	120100A_67	Subrounded	Euhedral	Medium
120100A_12	Subrounded	Euhedral	Medium	120100A_68	Subrounded	Euhedral	Medium
120100A_13	Subrounded	Euhedral	Medium	120100A_69	Angular	Euhedral	Medium
120100A_14	Subrounded	Euhedral	Small	120100A_70	Subrounded		Small
120100A_15	Subrounded		Medium	120100A_71	Subrounded		Small
120100A_16	Rounded		Large	120100A_72	Subrounded		Medium
120100A_17	Subrounded		Medium	120100A_73	Rounded		Medium
120100A_18	Subrounded		Medium	120100A_74	Subrounded		Medium
120100A_19	Rounded		Small	120100A_75	Rounded		Large
120100A_20	Rounded		Medium	120100A_76	Rounded		Medium
120100A_21	Rounded		Medium	120100A_77	Subrounded		Medium
120100A_22a	Rounded		Medium	120100A_78	Subrounded	Euhedral	Small
120100A_22b	Rim		Medium	120100A_79	Subrounded	Euhedral	Medium
120100A_23	Subrounded		Medium	120100A_80	Rounded		Small
120100A_24	Angular	Euhedral	Large	120100A_81	Subrounded		Large
120100A_25	Subrounded		Medium	120100A_82	Subrounded		Medium
120100A_26	Subrounded	Euhedral	Medium	120100A_83	Subrounded		Medium
120100A_27	Subrounded		Small	120100A_84	Subrounded		Medium
120100A_28	Subrounded	Euhedral	Medium	120100A_85	Rounded		Small
120100A_29	Subrounded		Small	120100A_86a	Subrounded	Euhedral	Medium
120100A_30	Subrounded	Euhedral	Medium	120100A_86b	Rim		Medium
120100A_31	Rounded		Small	120100A_87	Subrounded		Medium
120100A_32	Rounded		Small	120100A_88	Subrounded		Medium
120100A_33	Rounded		Small	120100A_89	Rounded		Small
120100A_34	Subrounded		Medium	120100A_90	Subrounded		Medium
120100A_35	Subrounded		Medium	120100A_91	Subrounded		Large
120100A_36	Subrounded	Euhedral	Medium	120100A_92	Subrounded		Medium
120100A_37	Subrounded		Large	120100A_93	Rounded		Medium
120100A_38	Rounded		Small	120100A_94	Rounded		Medium
120100A_39	Angular		Small	120100A_95	Subrounded		Small
120100A_40	Subrounded		Medium	120100A_96	Rounded		Medium
120100A_41	Subrounded	Euhedral	Medium	120100A_97	Subrounded	Euhedral	Medium
120100A_42	Subrounded		Medium	120100A_98	Rounded		Small
120100A_43	Rounded	Euhedral	Medium	120100A_99	Subrounded		Medium
120100A_44	Subrounded		Medium	120100A_100	Subrounded		Medium
120100A_45	Subrounded		Medium	120100A_101	Subrounded	Euhedral	Medium
120100A_46	Subrounded		Medium	120100A_102	Subrounded		Small
120100A_47	Subrounded		Medium	120100A_103	Subrounded		Medium
120100A_48	Rounded		Medium	120100A_104	Subrounded	Euhedral	Medium
120100A_49	Subrounded	Euhedral	Large	120100A_105	Subrounded		Small
120100A_50	Rounded	Euhedral	Medium	120100A_106	Rounded	Euhedral	Medium
120100A_51	Subrounded		Medium	120100A_107	Rounded		Small
120100A_52	Subrounded		Small	120100A_108	Subrounded		Small
120100A_53	Subrounded		Large	120100A_109	Subrounded	Euhedral	Medium
120100A_54	Subrounded	Euhedral	Medium	120100A_110	Rounded		Medium
120100A_55	Subrounded		Medium				

Appendix 2(8) Morphology of the zircon grains.

Sample ID	Description	Euhedral or not	Size	Sample ID	Description	Euhedral or not	Size
120112B_01	Rounded		Small	120112B_52	Rounded		Medium
120112B_02	Subrounded		Medium	120112B_53	Subrounded	Euhedral	Medium
120112B_03	Subrounded		Small	120112B_54	Rounded		Medium
120112B_04	Subrounded		Small	120112B_55	Subrounded		Medium
120112B_05	Subrounded		Large	120112B_56	Subrounded		Medium
120112B_06	Subrounded		Medium	120112B_57	Rounded		Medium
120112B_07	Subrounded		Medium	120112B_58	Rounded		Small
120112B_08	Rounded		Small	120112B_59	Subrounded	Euhedral	Medium
120112B_09	Angular		Small	120112B_60	Subrounded		Small
120112B_10	Angular		Medium	120112B_61	Rounded	Euhedral	Medium
120112B_11	Angular		Small	120112B_62	Rounded		Medium
120112B_12	Subrounded		Large	120112B_63	Subrounded	Euhedral	Medium
120112B_13	Subrounded		Medium	120112B_64	Subrounded	Euhedral	Medium
120112B_14	Angular		Small	120112B_65	Rounded		Small
120112B_15	Subrounded		Medium	120112B_66	Subrounded		Medium
120112B_16	Rounded		Large	120112B_67	Subrounded		Medium
120112B_17	Subrounded		Medium	120112B_68	Rounded		Medium
120112B_18	Subrounded		Medium	120112B_69	Subrounded		Medium
120112B_19	Subrounded		Medium	120112B_70	Subrounded		Medium
120112B_20	Rounded		Medium	120112B_71	Subrounded		Small
120112B_21	Subrounded		Medium	120112B_72	Subrounded		Medium
120112B_22	Subrounded		Medium	120112B_73	Subrounded	Euhedral	Medium
120112B_23	Subrounded	Euhedral	Small	120112B_74	Subrounded		Medium
120112B_24	Subrounded	Euhedral	Small	120112B_75	Subrounded		Medium
120112B_25	Subrounded		Medium	120112B_76	Subrounded	Euhedral	Medium
120112B_26	Subrounded		Medium	120112B_77	Angular		Medium
120112B_27	Subrounded	Euhedral	Medium	120112B_78	Subrounded		Medium
120112B_28	Subrounded		Medium	120112B_79	Rounded		Medium
120112B_29	Subrounded		Small	120112B_80	Subrounded		Medium
120112B_30	Subrounded		Medium	120112B_81	Angular		Large
120112B_31	Subrounded	Euhedral	Medium	120112B_82	Rounded		Medium
120112B_32	Rounded		Small	120112B_83	Subrounded		Small
120112B_33	Rounded		Small	120112B_84	Rounded		Medium
120112B_34	Subrounded		Medium	120112B_85	Rounded		Small
120112B_35	Subrounded		Medium	120112B_86	Rounded		Small
120112B_36	Angular		Medium	120112B_87	Subrounded		Medium
120112B_37	Subrounded		Medium	120112B_88	Subrounded		Medium
120112B_38	Subrounded		Large	120112B_89	Rounded	Euhedral	Medium
120112B_39	Subrounded		Large	120112B_90	Subrounded		Medium
120112B_40	Rounded		Medium	120112B_91	Angular		Small
120112B_41	Angular		Medium	120112B_92	Rounded		Small
120112B_42	Rounded		Medium	120112B_93	Subrounded		Medium
120112B_43	Subrounded	Euhedral	Small	120112B_94	Subrounded		Small
120112B_44	Subrounded		Medium	120112B_95	Rounded		Small
120112B_45	Subrounded		Medium	120112B_96	Subrounded	Euhedral	Medium
120112B_46	Rounded		Medium	120112B_97	Rounded		Large
120112B_47	Subrounded		Medium	120112B_98	Subrounded		Small
120112B_48	Rounded		Medium	120112B_99	Angular		Small
120112B_49	Rounded		Medium	120112B_100	Subrounded		Medium
120112B_50	Subrounded	Euhedral	Medium	120112B_101	Subrounded		Medium
120112B_51	Subrounded	Euhedral	Large				

Appendix 2(9) Morphology of the zircon grains.

Sample ID	Description	Euhedral or not	Size	Sample ID	Description	Euhedral or not	Size
120112C_01	Angular		Medium	120112C_52	Rounded		Medium
120112C_02	Rounded		Medium	120112C_53	Subrounded		Small
120112C_03	Subrounded		Medium	120112C_54	Subrounded		Medium
120112C_04	Subrounded	Euhedral	Small	120112C_55	Rounded	Euhedral	Large
120112C_05	Rounded		Medium	120112C_56	Rounded		Small
120112C_06a	Rounded	Euhedral	Large	120112C_57	Subrounded		Medium
120112C_06b	Rim		Large	120112C_58	Subrounded		Medium
120112C_07	Rounded		Medium	120112C_59	Subrounded	Euhedral	Medium
120112C_08	Subrounded	Euhedral	Small	120112C_60	Rounded		Small
120112C_09	Rounded		Medium	120112C_61	Angular		Medium
120112C_10	Subrounded	Euhedral	Small	120112C_62	Rounded		Small
120112C_11	Subrounded		Medium	120112C_63	Subrounded		Large
120112C_12	Subrounded		Medium	120112C_64	Rounded		Small
120112C_13a	Subrounded	Euhedral	Medium	120112C_65	Subrounded		Medium
120112C_13b	Rim		Medium	120112C_66a	Subrounded	Euhedral	Large
120112C_14	Subrounded	Euhedral	Medium	120112C_66b	Rim		Large
120112C_15	Subrounded		Medium	120112C_67	Subrounded		Medium
120112C_16	Subrounded		Medium	120112C_68	Rounded		Medium
120112C_17	Rounded		Large	120112C_69	Subrounded	Euhedral	Medium
120112C_18	Subrounded		Small	120112C_70	Rounded		Large
120112C_19	Subrounded		Small	120112C_71	Subrounded	Euhedral	Medium
120112C_20	Subrounded	Euhedral	Large	120112C_72	Subrounded	Euhedral	Medium
120112C_21	Subrounded	Euhedral	Medium	120112C_73	Subrounded	Euhedral	Medium
120112C_22	Subrounded		Medium	120112C_74	Subrounded		Medium
120112C_23	Subrounded		Medium	120112C_75	Subrounded	Euhedral	Medium
120112C_24	Subrounded		Medium	120112C_76	Subrounded		Small
120112C_25	Subrounded		Medium	120112C_77	Subrounded		Medium
120112C_26	Subrounded		Medium	120112C_78	Subrounded		Small
120112C_27	Angular		Small	120112C_79	Rounded		Medium
120112C_28	Subrounded		Small	120112C_80	Subrounded		Large
120112C_29	Rounded		Medium	120112C_81	Angular	Euhedral	Small
120112C_30	Rounded		Medium	120112C_82	Subrounded		Medium
120112C_31	Rounded		Medium	120112C_83	Rounded		Medium
120112C_32	Angular	Euhedral	Small	120112C_84	Subrounded		Small
120112C_33	Rounded		Small	120112C_85	Subrounded		Small
120112C_34	Subrounded		Medium	120112C_86	Subrounded		Medium
120112C_35	Subrounded		Medium	120112C_87	Subrounded		Medium
120112C_36	Subrounded	Euhedral	Medium	120112C_88	Rounded		Small
120112C_37	Subrounded	Euhedral	Medium	120112C_89	Subrounded	Euhedral	Large
120112C_38	Rounded		Small	120112C_90	Rounded	Euhedral	Medium
120112C_39	Rounded		Small	120112C_91	Subrounded		Medium
120112C_40	Subrounded		Small	120112C_92	Rounded		Small
120112C_41	Rounded		Medium	120112C_93	Subrounded		Small
120112C_42	Rounded		Small	120112C_94	Subrounded		Small
120112C_43	Subrounded		Small	120112C_95	Subrounded	Euhedral	Medium
120112C_44	Subrounded		Small	120112C_96	Rounded		Medium
120112C_45	Subrounded	Euhedral	Small	120112C_97	Angular		Medium
120112C_46	Rounded		Medium	120112C_98	Subrounded	Euhedral	Large
120112C_47	Angular	Euhedral	Medium	120112C_99	Subrounded	Euhedral	Large
120112C_48	Subrounded	Euhedral	Medium	120112C_100	Rounded		Medium
120112C_49	Rounded	Euhedral	Medium				
120112C_50	Rounded		Medium				
120112C_51	Rounded		Medium				

Appendix 3(3) U-Pb analyses.

Table with columns: Sample, Comment, Pb206/Pb204, 206Pb/(% Pb), Pb, Th, U, 207Pb/206Pb, 1s, 207Pb/235U, 1s, 206Pb/238U, 1s, % Concordance, Derived ages and errors (207Pb/206Pb 1s, 207Pb/235U 1s, 206Pb/238U 1s), T-W (Pbc corrected) (238U/206Pb 1s, 207Pb/206Pb 1s %).

Appendix 3(4) U-Pb analyses.

120063A_70	0	333511	0.0052	105	108	122	0.2214	0.0008	18.836	0.380	0.61	0.01	0.9	10	299	303	1	309	4	1.62055366	2.0	0.221381284	0.3
120063A_71	0	2621137	0.0007	654	292	1718	0.1166	0.0003	5.535	0.11	0.34	0.00	0.9	10	190	190	1	190	3	2.90365221	2.0	0.116567929	0.2
120063A_72	inclusions	6292	0.2736	99	48	293	0.1135	0.0004	4.763	0.098	0.30	0.00	0.9	9	185	177	1	171	3	3.28605774	2.0	0.113513012	0.3
120063A_73	0	480575	0.0036	131	119	252	0.1463	0.0005	8.675	0.173	0.43	0.00	0.9	10	230	230	1	230	3	2.32572981	2.0	0.146320174	0.3
120063A_74	0	725148	0.0024	203	145	315	0.1853	0.0006	13.270	0.267	0.51	0.01	0.9	10	270	269	1	269	4	1.92549680	2.0	0.185310447	0.3
120063A_75	0	213649	0.0081	59	32	87	0.1995	0.0007	15.248	0.308	0.55	0.01	0.9	10	282	283	1	284	4	1.80404930	2.0	0.199509725	0.3
120063A_76	0	635785	0.0027	158	65	407	0.1182	0.0004	5.744	0.118	0.35	0.00	0.9	10	192	193	1	194	3	2.83671950	2.0	0.118183625	0.3
120063A_77	0	361204	0.0048	97	115	226	0.1217	0.0005	6.067	0.123	0.36	0.00	0.9	10	198	198	1	199	3	2.76551024	2.0	0.121684312	0.3
120063A_78	0	324813	0.0053	90	119	199	0.1233	0.0005	6.272	0.127	0.36	0.00	0.9	10	200	201	1	202	3	2.70962069	2.0	0.123266292	0.3
120063A_79	0	529266	0.0033	140	142	342	0.1180	0.0004	5.688	0.115	0.34	0.00	0.9	10	192	193	1	193	3	2.86132848	2.0	0.118032942	0.3
120063A_80	0	117801	0.0146	35	33	51	0.1877	0.0008	13.568	0.278	0.52	0.01	0.9	10	272	272	1	271	4	1.90725483	2.0	0.187687512	0.4
120063A_81	0	113651	0.0151	35	79	89	0.1281	0.0008	6.462	0.132	0.37	0.00	0.9	10	204	204	1	203	3	2.89093810	2.0	0.128121153	0.4
120063A_82	0	182012	0.0095	55	76	88	0.1624	0.0007	10.492	0.213	0.48	0.00	0.9	10	248	247	1	247	4	2.13481045	2.0	0.162429406	0.4
120063A_83	0	528698	0.0033	144	188	310	0.1240	0.0004	6.568	0.133	0.38	0.00	0.9	10	201	209	1	209	3	2.80249854	2.0	0.123974539	0.3
120063A_84	0	147098	0.0117	43	78	91	0.1219	0.0006	6.157	0.126	0.36	0.00	0.9	10	198	199	1	201	3	2.72902917	2.0	0.121855819	0.3
120063A_85	0	297307	0.0058	74	27	192	0.1180	0.0005	5.711	0.116	0.35	0.00	0.9	10	192	193	1	193	3	2.8492529	2.0	0.118018967	0.4
120063A_86	0	254912	0.0068	69	82	156	0.1239	0.0005	6.302	0.128	0.36	0.00	0.9	10	201	201	1	202	3	2.71086503	2.0	0.12389635	0.4
120063A_87	0	655357	0.0026	188	159	295	0.1923	0.0006	13.308	0.268	0.50	0.01	0.9	9	276	270	1	262	4	1.9925615	2.0	0.192323121	0.3
120063A_88	0	351705	0.0049	111	300	234	0.1126	0.0005	5.281	0.107	0.34	0.00	0.9	10	184	186	1	188	3	2.94034202	2.0	0.112613682	0.4
120063A_89	0	280679	0.0081	70	31	184	0.1169	0.0005	5.571	0.113	0.34	0.00	0.9	10	190	191	1	191	3	2.89298209	2.0	0.116896178	0.4
120063A_90	0	183519	0.0094	50	89	150	0.1159	0.0006	4.416	0.090	0.27	0.00	0.9	8	189	171	1	157	2	3.61861406	2.0	0.11588679	0.5
120063A_91	0	288645	0.0064	79	79	116	0.1862	0.0007	13.502	0.273	0.52	0.01	0.9	10	270	271	1	272	4	1.90181430	2.0	0.18623869	0.3
120063A_92	0	39024	0.0441	10	12	26	0.1141	0.0011	5.393	0.118	0.34	0.00	0.9	10	186	186	1	190	3	2.91802388	2.0	0.114130156	0.3
120063A_93	0	157326	0.0109	46	85	95	0.1253	0.0005	6.464	0.132	0.37	0.00	0.9	10	203	204	1	204	3	2.67202854	2.0	0.125260363	0.4
120063A_94	0	413055	0.0042	126	162	183	0.1834	0.0006	12.916	0.260	0.51	0.01	0.9	9	268	267	1	266	4	1.95774324	2.0	0.183390617	0.3
120063A_95	0	648123	0.0027	169	157	431	0.1147	0.0004	5.359	0.109	0.33	0.00	0.9	10	187	187	1	188	3	2.9501258	2.0	0.11485558	0.3
120063A_96	0	124666	0.0138	34	40	81	0.1177	0.0008	5.662	0.116	0.34	0.00	0.9	10	192	192	1	193	3	2.8530578	2.0	0.117655819	0.4
120063A_97	0	892450	0.0019	240	303	596	0.1148	0.0004	5.349	0.108	0.33	0.00	0.9	10	187	187	1	188	3	2.9531519	2.0	0.114564499	0.3
120063A_98	0	781412	0.0022	208	120	404	0.1499	0.0005	9.044	0.182	0.43	0.00	0.9	10	234	234	1	234	3	2.28478748	2.0	0.149871087	0.3
120063A_99	0	652528	0.0026	183	129	289	0.1817	0.0006	12.800	0.258	0.51	0.01	0.9	10	266	266	1	266	4	1.95894270	2.0	0.181672116	0.3
120063A_100	0	364480	0.0047	98	94	217	0.1296	0.0005	6.793	0.137	0.38	0.00	0.9	9	209	208	1	207	3	2.63037522	2.0	0.12958806	0.3
120063A_101	0	379519	0.0045	96	57	248	0.1165	0.0004	5.574	0.113	0.34	0.00	0.9	10	190	191	1	192	3	2.88261851	2.0	0.116527952	0.3
120063A_102	0	704674	0.0024	170	10	457	0.1161	0.0004	5.594	0.113	0.34	0.00	0.9	10	189	191	1	193	3	2.86250973	2.0	0.116126853	0.3

Appendix 3(10) U-Pb analyses.

120097-120094_A_73		0	829161	0.0021	149	108	370	0.1184	0.0004	5.787	0.117	0.354	0.007	0.99	10	1933	6	1944	17	1955	34	2.82202666	2.00	0.118440133	0.33
120097-120094_A_74		0	1078561	0.0016	210	318	496	0.1171	0.0003	5.555	0.112	0.344	0.007	0.99	10	1912	5	1909	17	1906	33	2.905929633	2.00	0.1170761	0.29
120097-120094_A_75		0	243601	0.0071	54	76	73	0.1864	0.0007	13.542	0.274	0.527	0.011	0.98	10	2710	6	2718	19	2729	44	1.897349703	2.01	0.186554111	0.36
120097-120094_A_76		0	547468	0.0031	108	165	238	0.1221	0.0004	6.127	0.124	0.364	0.007	0.99	10	1987	6	1994	17	2001	34	2.747311671	2.00	0.122092634	0.33
120097-120094_A_77		0	546806	0.0031	116	210	225	0.1312	0.0004	6.947	0.140	0.384	0.008	0.99	99	2115	5	2105	18	2095	36	2.604723472	2.00	0.131238957	0.31
120097-120094_A_78		0	387008	0.0044	71	63	163	0.1257	0.0005	6.527	0.132	0.377	0.008	0.98	10	2039	7	2050	18	2060	35	2.655727561	2.01	0.125711542	0.40
120097-120094_A_79		0	226676	0.0076	41	33	101	0.1188	0.0005	5.799	0.117	0.354	0.007	0.98	10	1939	7	1946	17	1953	34	2.825371044	2.01	0.118838888	0.38
120097-120094_A_80		0	1500759	0.0011	276	236	646	0.1276	0.0004	6.468	0.130	0.368	0.007	0.99	98	2065	5	2042	18	2018	35	2.720097658	2.00	0.127605136	0.29
120097-120094_A_81	end of run	0	106850	0.0181	21	18	31	0.1921	0.0013	14.280	0.300	0.539	0.011	0.94	10	2761	11	2769	20	2779	46	1.855168122	2.04	0.192142971	0.70
120097-120094_A_82		0	156289	0.0110	29	32	72	0.1167	0.0005	5.562	0.113	0.346	0.007	0.98	10	1906	8	1910	17	1914	33	2.893132507	2.01	0.116709199	0.44
120097-120094_A_83	inclusions	0	163532	0.0105	31	28	86	0.1526	0.0008	6.336	0.130	0.301	0.008	0.97	7	2375	9	2023	18	1697	30	3.320573382	2.01	0.152688603	0.51
120097-120094_A_84		0	936573	0.0018	172	145	418	0.1169	0.0004	5.796	0.117	0.353	0.007	0.99	10	1940	6	1946	17	1951	34	2.829284649	2.00	0.116928276	0.32
120097-120094_A_85		0	461827	0.0031	90	56	140	0.1877	0.0006	13.490	0.274	0.521	0.010	0.99	99	2722	5	2715	19	2704	44	1.918708543	2.00	0.187720911	0.31
120097-120094_A_86		0	178842	0.0096	38	83	79	0.1219	0.0005	6.053	0.122	0.360	0.007	0.98	10	1984	7	1983	17	1983	34	2.776921867	2.01	0.121898761	0.38
120097-120094_A_87		0	268456	0.0064	48	29	120	0.1184	0.0004	5.783	0.117	0.354	0.007	0.98	10	1932	7	1944	17	1955	34	2.822927662	2.00	0.118396242	0.36
120097-120094_A_88		0	392539	0.0044	75	78	153	0.1358	0.0005	7.574	0.153	0.405	0.008	0.99	10	2174	6	2182	18	2190	37	2.471277415	2.00	0.135750654	0.33
120097-120094_A_89		0	1493200	0.0012	317	706	626	0.1281	0.0004	6.666	0.134	0.377	0.008	0.99	10	2072	5	2068	18	2064	35	2.649741556	2.00	0.128106638	0.29
120097-120094_A_90		0	69271	0.0249	12	8	31	0.1182	0.0006	5.673	0.117	0.348	0.007	0.96	10	1929	10	1927	18	1925	33	2.873333602	2.01	0.11821901	0.55
120097-120094_A_91		0	4041	0.4260	100	122	207	0.1278	0.0004	6.893	0.139	0.391	0.008	0.99	10	2068	6	2098	18	2129	36	2.555913547	2.00	0.127785364	0.34
120097-120094_A_92		0	582826	0.0030	108	115	295	0.1157	0.0004	4.985	0.100	0.313	0.006	0.99	99	1890	6	1817	17	1753	31	3.198336282	2.00	0.115668136	0.33
120097-120094_A_93		0	299314	0.0058	53	28	133	0.1205	0.0004	5.970	0.119	0.356	0.007	0.99	10	1963	6	1963	17	1962	34	2.810847543	2.00	0.120475603	0.34
120097-120094_A_94		0	914921	0.0019	205	544	413	0.1175	0.0004	5.685	0.119	0.351	0.007	0.99	10	1918	6	1929	17	1939	33	2.848985157	2.00	0.117477619	0.32
120097-120094_A_95		0	4414	0.3900	88	118	211	0.1145	0.0004	5.459	0.110	0.346	0.007	0.99	10	1872	6	1894	17	1915	33	2.891406883	2.00	0.114475122	0.35
120097-120094_A_96		0	4995	0.3447	95	172	218	0.1151	0.0004	5.439	0.110	0.343	0.007	0.99	10	1881	6	1891	17	1901	33	2.916399846	2.00	0.115051451	0.34
120097-120094_A_97		0	215409	0.0080	42	66	100	0.1170	0.0005	5.509	0.112	0.341	0.007	0.98	99	1911	7	1902	17	1894	33	2.928768455	2.01	0.117024848	0.40
120097-120094_A_98		0	310445	0.0055	60	82	140	0.1181	0.0004	5.732	0.118	0.352	0.007	0.98	10	1928	7	1936	17	1944	34	2.841514464	2.01	0.118129764	0.38
120097-120094_A_99		0	710206	0.0024	131	125	307	0.1231	0.0004	6.222	0.125	0.366	0.007	0.99	10	2002	5	2008	17	2013	35	2.728776533	2.00	0.123137877	0.31
120097-120094_A_100		0	1063693	0.0016	180	14	469	0.1182	0.0004	5.850	0.118	0.359	0.007	0.98	10	1930	7	1954	17	1977	34	2.786733666	2.00	0.118235766	0.37
120097-120094_A_101	short	0	58153	0.0031	100	61	256	0.1225	0.0005	5.837	0.118	0.346	0.007	0.98	98	1992	7	1952	17	1914	33	2.89228445	2.01	0.122450902	0.39
120097-120094_A_102		0	404448	0.0043	84	170	185	0.1181	0.0004	5.642	0.114	0.347	0.007	0.99	10	1928	6	1923	17	1918	33	2.86592809	2.00	0.118092749	0.35
120097-120094_A_103		0	131263	0.0131	25	28	62	0.1285	0.0005	5.802	0.118	0.333	0.007	0.98	90	2050	7	1947	17	1851	32	3.005789994	2.01	0.126492281	0.42
120097-120094_A_104		0	382323	0.0045	87	139	115	0.1895	0.0006	13.775	0.278	0.527	0.011	0.99	10	2738	5	2734	19	2730	44	1.896760769	2.00	0.189497722	0.33
120097-120094_A_105		0	1210	1.4232	20	13	28	0.1935	0.0009	14.859	0.302	0.557	0.011	0.98	10	2772	7	2806	19	2854	46	1.79569089	2.01	0.193515113	0.44
120097-120094_A_106		0	360743	0.0048	68	72	158	0.1186	0.0005	5.903	0.120	0.361	0.007	0.98	10	1936	7	1962	17	1986	34	2.77154452	2.01	0.118648088	0.39

Appendix 3(16) U-Pb analyses.

120112B_68	Inclusions	493734	0.0035	129	27	324	0.1219	0.0004	6.181	0.126	0.368	0.007	0.98	102	1984	8	2002	18	2019	35	2.719147196	2.01	0.121889043	0.43
120112B_69	0	268503	0.0064	72	40	181	0.1164	0.0005	5.754	0.117	0.358	0.007	0.98	104	1902	7	1939	17	1974	34	2.790353128	2.01	0.116440244	0.42
120112B_70	0	120669	0.0143	36	56	83	0.1186	0.0006	5.717	0.117	0.350	0.007	0.97	100	1936	9	1934	18	1932	33	2.860982461	2.01	0.118636643	0.50
120112B_71	0	1099619	0.0016	371	926	735	0.1222	0.0004	6.082	0.123	0.361	0.007	0.98	100	1989	6	1988	17	1988	34	2.771289052	2.00	0.122238806	0.36
120112B_72	0	80769	0.0213	23	25	56	0.1187	0.0007	5.738	0.118	0.351	0.007	0.98	100	1931	10	1937	18	1938	34	2.851765297	2.01	0.118688322	0.57
120112B_73	0	187967	0.0092	52	49	130	0.1173	0.0005	5.654	0.115	0.350	0.007	0.98	101	1919	8	1924	17	1933	33	2.860127447	2.01	0.117274354	0.44
120112B_74	0	187389	0.0092	51	33	131	0.1169	0.0006	5.549	0.114	0.344	0.007	0.97	100	1909	9	1908	18	1907	33	2.904255754	2.01	0.116879382	0.53
120112B_75	0	91850	0.0187	26	29	74	0.1168	0.0007	4.800	0.099	0.298	0.006	0.98	88	1906	10	1785	17	1681	30	3.356256568	2.01	0.116830719	0.56
120112B_76	0	451358	0.0038	118	39	314	0.1175	0.0005	5.625	0.115	0.347	0.007	0.97	100	1919	8	1920	17	1921	33	2.881037321	2.01	0.117530134	0.45
120112B_77	0	411947	0.0042	122	145	285	0.1182	0.0005	5.679	0.115	0.348	0.007	0.98	100	1923	8	1928	17	1927	33	2.869976426	2.01	0.118208788	0.43
120112B_78	Inclusions	268868	0.0065	81	60	144	0.1795	0.0007	11.110	0.225	0.449	0.009	0.98	90	2644	7	2532	19	2391	40	2.227408125	2.01	0.179479626	0.39
120112B_79	0	44083	0.0391	13	17	31	0.1182	0.0008	5.679	0.118	0.348	0.007	0.98	100	1931	12	1928	18	1927	34	2.870226905	2.02	0.118228417	0.65
120112B_80	0	212597	0.0081	59	53	141	0.1252	0.0006	6.282	0.128	0.364	0.007	0.97	99	2031	8	2018	18	2001	34	2.747589338	2.01	0.12517799	0.47
120112B_81	0	365358	0.0047	126	126	134	0.2618	0.0010	23.727	0.480	0.657	0.013	0.98	100	3258	6	3257	20	3256	51	1.521538434	2.01	0.261832577	0.37
120112B_82	0	232189	0.0074	75	168	163	0.1167	0.0005	5.537	0.113	0.344	0.007	0.98	100	1907	8	1908	17	1906	33	2.908359816	2.01	0.116718126	0.44
120112B_83	0	74124	0.0232	21	20	52	0.1173	0.0007	5.597	0.116	0.346	0.007	0.98	100	1919	11	1918	18	1916	33	2.8890906	2.01	0.117278443	0.59
120112B_84	0	481842	0.0036	147	54	245	0.2672	0.0010	17.509	0.354	0.475	0.010	0.98	76	3290	8	2963	19	2506	41	2.104298902	2.00	0.267221357	0.37
120112B_85	Inclusions	245148	0.0070	67	38	201	0.1175	0.0005	4.776	0.097	0.295	0.006	0.98	87	1913	7	1781	17	1666	29	3.391799743	2.01	0.11748059	0.42
120112B_86	0	428484	0.0040	128	180	326	0.1171	0.0005	5.129	0.104	0.318	0.006	0.98	93	1912	7	1841	17	1779	31	3.747304901	2.00	0.117068686	0.39
120112B_87	0	217374	0.0079	65	81	147	0.1208	0.0006	5.942	0.122	0.357	0.007	0.97	100	1968	9	1967	18	1967	34	2.803405843	2.01	0.120807437	0.49
120112B_88	0	167853	0.0103	56	72	74	0.1986	0.0009	14.944	0.304	0.546	0.011	0.98	100	2819	7	2812	19	2808	46	1.832190738	2.01	0.198581729	0.45
120112B_89	0	93749	0.0184	29	32	46	0.1764	0.0008	12.105	0.247	0.498	0.010	0.97	99	2620	8	2613	19	2603	43	2.009760587	2.01	0.176439586	0.47
120112B_90	0	175471	0.0098	85	189	115	0.1250	0.0006	6.365	0.130	0.369	0.007	0.97	100	2022	9	2021	18	2028	35	2.708245618	2.01	0.125023182	0.49
120112B_91	0	215291	0.0080	64	107	151	0.1174	0.0005	5.581	0.114	0.345	0.007	0.98	100	1917	8	1913	17	1910	33	2.899482748	2.01	0.117371604	0.45
120112B_92	0	342368	0.0050	103	168	240	0.1172	0.0005	5.585	0.114	0.346	0.007	0.98	100	1914	8	1914	17	1914	33	2.892987165	2.01	0.117188963	0.43
120112B_93	0	113539	0.0152	34	22	55	0.1887	0.0010	12.907	0.265	0.496	0.010	0.97	99	2731	9	2673	19	2597	43	2.015768104	2.01	0.188701238	0.53
120112B_94	Inclusions	208184	0.0083	66	113	158	0.1237	0.0006	5.430	0.111	0.318	0.006	0.97	89	2010	9	1890	17	1782	31	3.140540722	2.01	0.12367188	0.49
120112B_95	0	119199	0.0144	33	26	79	0.1240	0.0007	6.218	0.128	0.364	0.007	0.97	99	2019	9	2007	18	1999	34	2.750344883	2.01	0.124040827	0.53
120112B_96	0	85064	0.0202	28	34	47	0.1864	0.0010	11.162	0.229	0.434	0.009	0.97	88	2710	9	2537	19	2326	39	2.302014992	2.01	0.186366299	0.53
120112B_97	0	247011	0.0070	78	128	176	0.1159	0.0008	5.429	0.111	0.340	0.007	0.97	100	1894	9	1883	17	1885	33	2.943927606	2.01	0.115922188	0.50
120112B_98	0	282354	0.0061	87	143	189	0.1196	0.0006	5.954	0.122	0.361	0.007	0.97	102	1951	8	1968	18	1987	34	2.77063698	2.01	0.119634233	0.47
120112B_99	0	115949	0.0148	33	34	77	0.1233	0.0006	6.203	0.127	0.365	0.007	0.97	100	2004	9	2005	18	2005	35	2.740257144	2.01	0.123274924	0.50
120112B_100	0	315793	0.0055	88	78	224	0.1159	0.0005	5.459	0.111	0.342	0.007	0.98	100	1893	7	1894	17	1895	33	2.826300968	2.01	0.115865492	0.41
120112B_101	Inclusions	102720	0.0168	29	29	99	0.1176	0.0007	4.063	0.084	0.251	0.005	0.98	75	1920	11	1647	17	1442	26	3.990202346	2.01	0.117593906	0.63

Appendix 3(18) U-Pb analyses.

120112C_67	0	484693	0.0036	128	113	347	0.1162	0.0005	5.114	0.104	0.319	0.006	0.98	94	1899	7	1838	17	1784	31	3.133869695	2.00	0.116234181	0.39
120112C_68	0	107316	0.0160	30	17	42	0.2158	0.0011	17.299	0.355	0.581	0.012	0.97	100	2950	8	2952	19	2954	48	1.719961514	2.02	0.21578745	0.51
120112C_69	0	236893	0.0073	63	63	157	0.1166	0.0005	5.520	0.113	0.343	0.007	0.97	100	1905	8	1904	17	1903	33	2.912205991	2.01	0.116588231	0.47
120112C_70	0	543437	0.0032	134	41	360	0.1177	0.0004	5.601	0.113	0.345	0.007	0.98	99	1922	7	1918	17	1911	33	2.898334031	2.00	0.117740523	0.38
120112C_71	0	274897	0.0063	69	33	169	0.1253	0.0006	6.398	0.130	0.370	0.007	0.98	100	2033	8	2032	18	2031	35	2.700145679	2.01	0.125290082	0.44
120112C_72	0	424064	0.0041	105	37	282	0.1174	0.0005	5.561	0.113	0.344	0.007	0.98	99	1917	7	1910	17	1904	33	2.910478207	2.00	0.117391763	0.40
120112C_73	0	383929	0.0045	100	99	255	0.1166	0.0005	5.519	0.112	0.343	0.007	0.98	100	1905	7	1904	17	1902	33	2.914056489	2.00	0.116636515	0.40
120112C_74	0	398387	0.0043	107	64	190	0.1537	0.0006	10.135	0.206	0.478	0.010	0.98	106	2388	7	2407	19	2519	42	2.091211838	2.01	0.153709556	0.40
120112C_75	0	483592	0.0036	135	87	206	0.1929	0.0007	14.232	0.288	0.535	0.011	0.98	100	2767	6	2765	19	2763	45	1.868478371	2.00	0.192871451	0.37
120112C_76	0	622368	0.0028	169	87	288	0.1827	0.0007	12.430	0.251	0.493	0.010	0.98	97	2678	6	2637	19	2585	43	2.026666647	2.00	0.182704129	0.36
120112C_77	0	533233	0.0032	151	298	508	0.1106	0.0005	3.658	0.074	0.240	0.005	0.98	77	1809	7	1562	16	1381	25	4.167208877	2.00	0.110553968	0.41
120112C_78	step in rat	95297	0.0131	27	17	37	0.2048	0.0010	16.724	0.342	0.592	0.012	0.97	105	2835	8	2919	19	2991	48	1.688159845	2.01	0.204760543	0.47
120112C_79	inclusions	578402	0.0030	148	56	348	0.1170	0.0005	6.133	0.125	0.380	0.008	0.99	109	1912	8	1995	18	2074	36	2.831425488	2.01	0.117048024	0.43
120112C_80	0	109471	0.0157	32	55	68	0.1299	0.0006	6.580	0.134	0.367	0.007	0.97	96	2097	8	2057	18	2011	35	2.722549325	2.01	0.129925325	0.48
120112C_81	0	1961	0.8778	82	161	93	0.1202	0.0006	5.914	0.121	0.357	0.007	0.97	100	1959	8	1963	18	1964	34	2.801588334	2.01	0.120162824	0.47
120112C_82	0	683051	0.0025	222	330	295	0.1852	0.0007	13.502	0.274	0.529	0.011	0.98	101	2700	6	2715	19	2736	45	1.891051949	2.00	0.18518293	0.39
120112C_83	0	133192	0.0129	37	54	86	0.1198	0.0006	5.816	0.119	0.352	0.007	0.97	100	1953	8	1949	18	1945	34	2.839460795	2.01	0.11976762	0.47
120112C_84	0	937742	0.0018	240	136	570	0.1261	0.0005	6.535	0.132	0.376	0.008	0.98	101	2044	7	2051	18	2057	35	2.65990152	2.00	0.126064248	0.38
120112C_85	0	391294	0.0044	114	109	182	0.1780	0.0007	12.054	0.244	0.491	0.010	0.98	98	2635	6	2609	19	2574	42	2.036603337	2.00	0.178046209	0.39
120112C_86	0	280897	0.0061	77	138	285	0.1113	0.0005	3.459	0.070	0.225	0.005	0.98	72	1821	8	1518	16	1311	24	4.437645631	2.01	0.111335105	0.42
120112C_87	short	544844	0.0032	163	325	344	0.1268	0.0005	6.342	0.129	0.365	0.007	0.98	97	2055	8	2024	18	1994	34	2.757659994	2.01	0.126839599	0.43
120112C_88	0	257284	0.0067	72	100	166	0.1191	0.0005	5.832	0.119	0.355	0.007	0.97	101	1943	8	1951	18	1958	34	2.816567465	2.01	0.119143286	0.46
120112C_89	0	187504	0.0092	47	24	123	0.1186	0.0005	5.708	0.116	0.349	0.007	0.98	100	1935	8	1933	17	1930	33	2.864211364	2.01	0.118580878	0.45
120112C_90	0	147219	0.0117	41	46	89	0.1273	0.0006	6.623	0.136	0.377	0.008	0.97	100	2061	9	2062	18	2064	35	2.650074456	2.01	0.127302205	0.50
120112C_91	0	344854	0.0050	97	133	225	0.1200	0.0005	5.811	0.118	0.351	0.007	0.98	99	1956	7	1948	17	1944	34	2.846853221	2.00	0.119982197	0.40
120112C_92	0	209642	0.0082	57	55	118	0.1275	0.0007	7.255	0.149	0.413	0.008	0.97	108	2083	9	2143	18	2228	38	2.422454637	2.01	0.127464403	0.53
120112C_93	0	102058	0.0189	28	40	69	0.1163	0.0006	5.434	0.111	0.339	0.007	0.97	99	1900	9	1890	17	1881	33	2.950574478	2.01	0.116275186	0.51
120112C_94	0	168808	0.0102	44	40	111	0.1172	0.0005	5.823	0.115	0.348	0.007	0.98	101	1915	8	1920	17	1924	33	2.874528891	2.01	0.117235548	0.45
120112C_95	0	105633	0.0163	29	37	70	0.1169	0.0006	5.595	0.115	0.347	0.007	0.96	101	1910	10	1915	18	1920	33	2.881950337	2.01	0.116945906	0.55
120112C_96	0	298943	0.0058	78	64	192	0.1178	0.0005	5.801	0.118	0.357	0.007	0.98	102	1923	8	1947	17	1965	34	2.800598645	2.01	0.117824912	0.44
120112C_97	0	235563	0.0073	63	57	147	0.1235	0.0006	6.260	0.128	0.368	0.007	0.97	101	2007	9	2013	18	2016	35	2.720301088	2.01	0.12350652	0.49
120112C_98	0	176153	0.0098	49	63	105	0.1293	0.0006	6.844	0.140	0.384	0.008	0.97	100	2088	8	2091	18	2098	36	2.604338357	2.01	0.129281595	0.48
120112C_99	0	494508	0.0035	122	37	320	0.1190	0.0005	5.804	0.118	0.354	0.007	0.98	101	1941	8	1947	17	1953	34	2.826282523	2.01	0.118980425	0.43
120112C_100	0	219911	0.0078	58	47	137	0.1230	0.0006	6.233	0.127	0.368	0.007	0.97	101	2000	8	2009	18	2014	35	2.720907023	2.01	0.12298183	0.46